Current Research in Food Science 10 (2025) 101084

Contents lists available at ScienceDirect

Current Research in Food Science

journal homepage: www.sciencedirect.com/journal/current-research-in-food-science

Gallic acid prevents obesity in mice on a high-fat diet via the gut microbiota-adipose tissue axis

Shiyan Jian [a,1], Xiaoying Jian [a,1], Lan Ye [a,1], Kang Yang [b], Limeng Zhang [c], Yixuan Xie [a], Jinping Deng [a], Yulong Yin [d], Baichuan Deng [a,*]

[a] Guangdong Provincial Key Laboratory of Animal Nutrition Control, College of Animal Science, South China Agricultural University, Guangzhou, 510642, China
[b] School of Life and Health Science, Kaili University, Kaili, 556011, China
[c] Guangzhou Qingke Biotechnology Co., Ltd., Guangzhou, 510475, Guangdong, China
[d] Institute of Subtropical Agriculture, Chinese Academy of Sciences, Changsha, 410125, China

ARTICLE INFO

Handling Editor: Dr. Quancai Sun

Keywords:
Obesity
Gallic acid
High-fat diet
Gut microbiota
Gut microbiota-adipose tissue axis

ABSTRACT

Obesity is closely related to the gut microbiota, and gallic acid (GA) has anti-obesity properties, but its relationship with the gut microbiota is unclear. The aim of this study was to investigate the role of gut microbiota in the anti-obesity mechanism of GA by fecal microbiota transplantation (FMT). Here, we found that high-fat diet (HFD) promoted lipid deposition and gut microbiota dysbiosis in mice, whereas GA slowed down lipid deposition and restored gut microbiota dysbiosis and its functional profile, as evidenced by the reduction of the obesity-causing bacterium *Desulfovibrio* and the enrichment of the beneficial bacterium *Lachnospiraceae_NK4A136_group*, *Clostridiales_unclassified*, *Oscillospira* and *Adlercreutzia*. These gut microbiota and metabolites produced positive feedback effects on body weight, glucose tolerance, insulin resistance, as well as glycemic and lipid parameters. Mechanistically, GA significantly enhanced lipid and energy metabolism in obese mice by promoting the expression of uncoupling protein 1 (UCP1), adiponectin, and adiponectin receptor 2 in white adipose tissue of the epididymal white adipose tissue, as well as promoting thermogenesis in interscapular brown adipose tissue by stimulating UCP1 expression. Interestingly, GA failed to alleviate lipid accumulation in HFD of antibiotic-treated mice. In contrast, after FMT treatment, the fecal microbiota of GA-treated donor mice significantly alleviated lipid metabolism in HFD-fed mice, which is mechanistically consistent with direct addition of GA. Collectively, GA can alleviate HFD-induced obesity by modulating the gut microbiota, and the specific mechanism may be through the gut microbiota-adipose tissue axis.

1. Introduction

The prevalence of obesity, particularly the subtype stemming from dietary factors known as diet-induced obesity (DIO), constitutes a substantial threat to both severe morbidity and elevated mortality rates due to the widespread consumption of high-fat diets (Lingvay et al., 2022), underscores the urgency for comprehensive strategies to address this growing concern (Perdomo et al., 2023). In recent times, a considerable accumulation of data has shone a light on the central significance of gut microbiota dysbiosis in the emergence and progression of obesity (Li et al., 2021) along with its comorbidities, inclusive of type 2 diabetes, cardiovascular disorders (Piché et al., 2020), hyperlipidemia (González-Domínguez et al., 2023), and fatty liver disease (Muzurovic et al., 2022), emphasizing the imperative need for targeted interventions to redress this microbial imbalance. The disturbance of energy equilibrium, instigated by gut microbiota dysbiosis as a consequence of high-fat diet (HFD), has been documented to initiate low-grade persistent inflammation and impair intestinal barrier integrity, ultimately contributing to the establishment of obesity (Dalby et al., 2017; Wang et al., 2020a). Hence, embracing dietary alterations designed to regulate the gut microbiota presents a promising strategy for combating obesity (Santos-Marcos et al., 2019).

Recent investigations have proposed the potential benefits of incorporating functional food additives, such as resveratrol (Wang et al.,

* Corresponding author. Guangdong Provincial Key Laboratory of Animal Nutrition Control, College of Animal Science, South China Agricultural University, Guangzhou 510642, China.
E-mail address: dengbaichuan@scau.edu.cn (B. Deng).
[1] These authors contributed equally to this work.

https://doi.org/10.1016/j.crfs.2025.101084
Received 20 December 2024; Received in revised form 5 April 2025; Accepted 15 May 2025
Available online 16 May 2025

2020b) and curcumin (Li et al., 2021) into obesity intervention strategies. These compounds are suggested to exert a modulating effect on the gut microbiota, offering a promising approach in the fight against obesity. Recently, there has been a growing emphasis on exploring functional food-derived compounds as viable dietary interventions for enhancing physiological outcomes and mitigating pathological consequences associated with obesity (Jian et al., 2023). The aforementioned constituents possess the capability to directly modulate the expression of host genes that govern obesity-related phenotypic attributes, thereby offering a targeted approach to address the underlying mechanisms of obesity (Liu et al., 2020). Plant-derived polyphenol compounds exhibit various pharmacological properties, such as anti-aging (Guo et al., 2022), antibacterial (Mithul Aravind et al., 2021), anti-inflammatory, and antioxidant properties (Truong and Jeong, 2022). In addition, only 5 %–10 % of polyphenol compounds are absorbed by the small intestine, with the rest passing into the large intestine and being excreted in feces (Mithul Aravind et al., 2021). Thus, it is hypothesized that polyphenols mainly exert their multiple functions through gut microbiota and its related metabolites (Breton et al., 2016; Tian and Jin, 2016; Wang et al., 2012; Wu et al., 2021).

Gallic acid (3,4,5-trihydroxybenzoic acid, GA) is a polyphenol compound with anti-inflammatory, antioxidant, anticancer, and antibacterial activities (Yang et al., 2020). GA has been established as a safe and well-tolerated compound, even at elevated dosages, exemplified by its administration at 900 mg/kg in murine models, without eliciting adverse effects (Huber et al., 2006) and 1000 μM in Neutrophils cells (Li et al., 2019). Accumulating evidence from research endeavors has demonstrated the efficacy of GA in preventing and/or mitigating a plethora of chronic ailments linked to obesity, notably non-alcoholic fatty liver disease, diabetes mellitus, and non-alcoholic steatohepatitis, underscoring its potential as a therapeutic agent against obesity-related complications (Chao et al., 2021), hypertriglyceridemia (Huang et al., 2018), atherosclerosis, and vascular senescence (Clark et al., 2022). To date, GA has also been reported to have beneficial anti-obesity effects, but the available studies have not yet elucidated its specific mechanisms (Bak et al., 2013; Dludla et al., 2018; Umadevi et al., 2014). Prior studies have indicated the thermogenic capability of GA on brown adipose tissue (BAT), while simultaneously diminishing lipid deposition in white adipose tissue (WAT), thus proposing a dual mechanism by which GA may contribute to the management of obesity (Doan et al., 2015; Paraíso et al., 2019a). Emerging evidence suggests the potential of GA to affect the microbiota through its ability to increase beneficial bacterial populations and stimulate the biosynthesis of SCFAs. Preclinical studies demonstrate the ability of GA to restore gut microbial ecology disrupted by obesity, with particular efficacy in restoring *Erysipelatoclostridium* and *Eubacterium* populations in mouse models (Peng et al., 2024). Remarkably, GA intervention significantly increased both species-specific and total SCFA levels in all species, as evidenced by increased acetic acid production in canines and increased fecal triglyceride excretion in HFD rats via modulation of the microbiota-gut-brain-liver axis (Yang et al., 2022a; Chang et al., 2024). Mechanistic studies revealed dual regulatory effects, including inhibition of α-glucosidase activity, reduction of the Firmicutes/Bacteroidetes ratio, and selective enrichment of SCFA-producing genera (i.e., *Allobaculum* and *Bifidobacterium*) (Dou et al., 2022). These microbiological shifts correlated strongly with improvements in metabolic parameters-in particular increased insulin receptor expression and attenuated leptin resistance (Chang et al., 2024). In particular, the therapeutic potential extends to polyherbal formulations in which GA is the major bioactive component, demonstrating sustained efficacy in the treatment of diabetes through consistent SCFA-mediated mechanisms (Singh et al., 2024). However, although the anti-obesity effect of GA has been well established, the complex interactions between its therapeutic efficacy and gut microbial ecology remain under characterized. Therefore, the present study aimed to elucidate the mechanistic basis of the anti-obesity activity of GA by systematically investigating the therapeutic modulation of GA by the gut microbiota-adipose tissue axis.

Here, we explored the anti-obesity effects of GA in mice on a HFD and also investigated the effects of GA on the gut microbiota and microbiota metabolism in HFD-fed mice. In addition, by removing the gut microbiota in HFD-fed mice, we also explored whether GA still has anti-obesity capacity. Finally, we confirmed whether GA exerts its anti-obesity effects through gut microbes by transplanting gut microbiota from GA-treated HFD-fed mice. We hypothesized that HFD-induced disruption of the gut microbiota induces obesity, and that GA would exert an anti-obesity effect by modulating the gut microbiota in mice.

2. Materials and methods

2.1. Materials and diets

GA was purchased from Wufeng Chicheng Biotech Co., Ltd. (Yichnag, China). The chow diet, which derived 13.5 % of its energy from fat and was designated as XTADG001, and the HFD, obtaining 60 % of its energy content from fat and labeled as XTHF60, were both obtained from Xietong Pharmaceutical Bio-engineering Co., Ltd., located in Jiangsu, China. The detailed compositions of both the normal diet and the HFD are presented in Table S1.

2.2. Animals and experimental design

The animals in this study consisted of specific pathogen-free four-week-old male C57BL/6 J mice, sourced from the Guangdong Medical Laboratory Animal Center in Guangzhou, China, under the authorization number SYXK (Yue) 2019–0136. Ethical approval for all animal procedures detailed herein was granted by the Experimental Animal Ethics Committee of South China Agricultural University (Approval number: 2022F233). Throughout the experimental period, all mice were provided with unrestricted access to both food and water. They were housed within a controlled environment, maintained at a temperature of 25 ± 2 °C, a relative humidity ranging from 45 % to 60 %, and a lighting cycle of 12 h per day (08:00–20:00 for light). GA was incorporated into the HFD in proportion to the individual food intake of mice. The weekly food consumption and body weight of each mouse were meticulously recorded.

2.2.1. Experiment 1

After a 1-week adaptation period, thirty mice (17.72 ± 0.99 g) were allocated at random into three distinct groups (n = 10) based on body weight: normal chew diet (CON), HFD, and HFD along with 200 mg/kg body weight of GA (HFD + GA). The dosage of 200 mg/kg body weight for the GA treatment was informed by the findings from our pre-experiment results (Fig. S1). Body composition, non-shivering thermogenesis, and basal metabolic rate were examined in all mice at week 7 and week 8. At the week 7 and week 8, respectively, an IPGTT and an IPITT were conducted. Subsequently, all mice were anaesthetized with isoflurane to facilitate sampling. Blood samples were gathered for the biochemical analysis. Additionally, the inguinal subcutaneous white adipose tissue (iWAT), epididymal white adipose tissue (eWAT), perirenal white adipose tissue (pWAT), and interscapular brown adipose tissue (iBAT) were carefully weighed and subsequently collected. Colonic contents were collected for 16 S rRNA sequencing, and fresh feces were used for untargeted and targeted metabolomics analysis.

2.2.2. Experiment 2

For antibiotic treatment, thirty mice (17.93 ± 1.23 g) were allocated at random into three distinct groups (n = 10) based on body weight: HFD, HFD combined with antibiotics treatment (HFD + Abx), and HFD along with antibiotics plus additional 200 mg/kg body weight of GA (HFD + Abx + GA). Mice assigned to the HFD group received HFD accompanied by sterile water. Conversely, mice in both the HFD + Abx and HFD + Abx + GA groups underwent treatment with antibiotics,

including 1 g/L streptomycin (MedChemExpress, HY-B0472), 1 g/L ampicillin (MedChemExpress, HY-B0522), 1 g/L gentamicin (MedChemExpress, HY-A0276A), and 0.5 g/L vancomycin (MedChemExpress, HY-B0671) dissolved in sterile water to obtain the pseudo-germfree mice, in addition to the HFD. Drinking water was measured each morning to ensure adequate antibiotic consumption, and new drinking water intake was prepared every 3 days. Confirmation of gut microbiota depletion was achieved through the analysis of fecal DNA levels. At the week 7 and week 8, respectively, an IPGTT and an IPITT were conducted. Subsequently, all mice were anaesthetized with isoflurane to facilitate sampling. The iWAT, eWAT, pWAT, and iBAT samples were weighed.

2.2.3. Experiment 3

In the fecal microbiota transplantation (FMT), twenty donor mice (17.64 ± 1.36 g) were allocated at random into two distinct groups (n = 10) based on body weight: HFD and HFD + GA. Continuous daily fecal collection was started after 7 weeks for 1 week. Feces are collected and preserved as described in previous reports (Barcena et al., 2019). Briefly, A suspension of 200 mg of fresh fecal pellets was prepared in 2.0 mL of anaerobic PBS. This suspension was subsequently centrifuged at 100 *g* for a duration of 1 min, aiming to eliminate insolubilized material, and 10 % sterile glycerol was added to the fecal suspension. The sealed centrifuge tube was stored at −80 °C. Afterwards, the supernatant was gathered and administered to the recipient mice via oral gavage, with each mouse receiving 200 μL every two days. The recipient mice were divided into two groups through random assignment (n = 10): one receiving FMT from the HFD (FMT-HFD), and the other receiving FMT from HFD group plus 200 mg/kg body weight of GA (FMT-HFD + GA). The mice belonging to both the FMT-HFD and FMT-HFD + GA groups were provided with HFD. All recipient mice were pretreated with antibiotics, consisting of 1 g/L streptomycin (MedChemExpress, HY-B0472), 1 g/L ampicillin (MedChemExpress, HY-B0522), 1 g/L gentamicin (MedChemExpress, HY-A0276A), and 0.5 g/L vancomycin (MedChemExpress, HY-B0671), dissolved in sterile water for 2 weeks to obtain pseudo germ-free mice (Barcena et al., 2019; Yin et al., 2018). Antibiotics were monitored daily to ensure adequate intake, and new drinking water was prepared every 2 days. Confirmation of gut microbiota depletion was achieved through the analysis of fecal DNA levels. Following a 6-week transplantation period, body composition, non-shivering thermogenesis, and basal metabolic rate were examined in all mice at the week 6. And the recipient mice were anaesthetized using isoflurane prior to sampling. Subsequently, blood samples were gathered for biochemical analysis. The iWAT, eWAT, pWAT, and iBAT samples were weighed and collected. Colonic contents were collected for 16 S rRNA sequencing, and fresh feces were used for untargeted metabolomics analysis.

2.3. Body composition

The body fat content and distribution of the mice were evaluated utilizing a small animal body composition analysis and imaging system, specifically the MRI analyzer (MesoQMR23-060H, Niumag Corporation, Shanghai, China), as previously described in the literature (Yang et al., 2022b).

2.4. Cold exposure and body temperature monitoring

Cold exposure is induced by placing mice at 25 °C (initial temperature) in cages maintained at 4 °C (cold exposure temperature) for 6 h. During this process, food but not water was withheld. Subsequently, the temperature of the iBAT was monitored by employing an infrared thermal detection device (FLIR, America), while the rectal temperature was measured using an anal thermometer (ALC-ET03, Shanghai Alcott Biotech Co., Ltd., China).

2.5. Basal metabolic rate

The metabolic parameters of mice were assessed utilizing a comprehensive lab animal monitoring system, known as CLAMS (Promethion Metabolic Screening Systems, Sable Systems International, North Las Vegas, NV, USA), over a 24-h period starting at 18:00. The average values for the mean energy expenditure (mean EE) and respiratory exchange ratio (RER) were determined and examined.

2.6. Intraperitoneal glucose tolerance test

After a period of 12 h of fasting, the mice were administered an IPGTT with a glucose dose of 2 g/kg body weight. Blood glucose levels were measured in the tail vein blood at specific time points: 0, 15, 30, 60, 90, and 120 min following the intraperitoneal administration of glucose. To assess the outcomes of the IPGTT quantitatively, the trapezoidal method was employed for calculating the area under the curve (AUC), providing a comprehensive measure of glucose response.

2.7. Intraperitoneal insulin tolerance test

After a 6-h fasting period, the mice underwent an IPITT with an insulin dose of 0.75 UI/kg body weight (GlpBio, USA). Blood glucose levels were then measured in the tail vein blood at 0, 15, 30, 60, 90, and 120 min following the intraperitoneal administration of insulin. To assess the outcomes of the IPITT quantitatively, the trapezoidal method was employed for calculating the AUC, providing a comprehensive measure of glucose response.

2.8. Histological analysis

The duodenum and eWAT samples were preserved using 10 % formalin, subsequently embedded in paraffin, and sectioned into slices of 5 μm thickness. These sections were then stained with hematoxylin and eosin (H&E). The Nikon Eclipse E100 microscope (Nikon, Tokyo, Japan) was utilized to analyze the villus length and crypt depth of the duodenum, while the adipocyte area of the eWATs was quantified using Image-Pro Plus 6.0 software (Media Cybernetics, MD, USA).

2.9. Biochemical analysis

The concentrations of serum glucose (Glu), total cholesterol (TC), triglyceride (TG), low-density lipoprotein cholesterol (LDL-C), high-density lipoprotein cholesterol (HDL-C), lipopolysaccharides (LPS), total bile acid (TBA), and lipase were determined using commercially available assay kits sourced from the Nanjing Jiancheng Bioengineering Institute, located in Nanjing, China.

2.10. Quantitative real-time PCR

The RNA from the eWAT samples was extracted utilizing the Adipose Tissue Purification Kit provided by EZBioscience (California, USA). Subsequently, the isolated RNA was converted into cDNA following the reversal protocol outlined in the 4 × EZscript Reverse Transcription Mix II supplied by EZBioscience (California, USA). The cDNA was then analyzed on an ABI QuantStudio 6 Flex system (Applied Biosystems, Carlsbad, CA) in combination with SYBR Green qPCR SuperMix (EZBioscience, California, USA). The β-actin served as the housekeeping gene for normalization purposes, and the mRNA expression levels were calculated using the 2-ΔΔCt method. The qRT-PCR primer sequences utilized in this study are presented in Table S2.

2.11. Western blotting analysis

Initially, the protein from the eWAT samples was lysed using RIPA lysis buffer (P70100, NCM Biotech, China). Subsequently, the protein

content was quantified employing BCA protein assay reagent (P0012, BIOTIME, China). Subsequently, an equal quantity of protein derived from the respective samples was fractionated via electrophoresis, utilizing a 10 % polyacrylamide gel electrophoresis (PAGE) system fortified with sodium dodecyl sulfate (SDS) for optimal separation (Sle 020, Smart-Lifescience, China). Following this, the proteins were transferred onto polyvinylidene difluoride (PVDF) membranes (BS-PVDF-45-S, Biosharp, China) and incubated with 5 % skimmed milk powder for a duration of 2 h. After the incubation, the membranes were treated with primary antibodies against uncoupling protein 1 (UCP1; diluted 1:1000), adiponectin (AdipoQ; diluted 1:2000), adiponectin receptor 2 (AdipoR2; diluted 1:2000), and β-actin (diluted 1:6000), followed by the application of secondary antibodies. The proteins were then visualized using luminescent reagent P10200 (NCM Biotech, China). The generated chromogenic bands were quantified and subsequently standardized relative to β-actin levels, employing the Image Lab software for consistent analysis. Details regarding the primary antibodies utilized in this study are presented in Table S3. Western blot images are provided in Fig. S5.

2.12. Immunohistochemistry

In summary, following deparaffinization and antigen retrieval, the eWAT tissues underwent fixation, sectioning, and blocking of proteins as well as endogenous enzymes. Subsequently, they were incubated with both primary and secondary antibodies. The nuclei were then stained multiple times using diaminobenzidine and hematoxylin, before being dehydrated and mounted for microscopic analysis with the aid of ImageJ software.

2.13. Immunofluorescence

Briefly, the eWAT tissues were deparaffinized, hydrated, antigenically repaired, and sealed with 3 % hydrogen peroxide solution, the sealing solution was discarded. Afterwards, the primary antibody was added dropwise and incubated and incubated with HRP-Polymer secondary antibody, and then the nuclei of the cells were re-stained using the 570-tyramide signal amplification (TSA) marker and dropwise 4ʼ,6-diamidino-2-phenylindole (DAPI), and finally fluorescently sealed and microscopically examined. The nuclei were stained with 570-TSA and DAPI, and finally, the cells were fluorescently blocked and examined by microscopy.

2.14. Gut microbiota analysis

The isolation of genomic DNA from colonic content specimens was carried out as a preliminary step using the E. Z.N.A.® Stool DNA Kit (Omega Bio-tek, Norcross, GA, U.S.). Additionally, the quality of the extracted DNA was evaluated utilizing agarose gel electrophoresis, ensuring its suitability for downstream applications, while DNA was quantified by UV spectrophotometer. To amplify the V3+V4 hypervariable region of the 16 S rRNA, the PCR reaction utilized the specific primers 515 F (5′-GTGYCAGCMGCCGCGGTAA-3′) and 805 R (5′-GGACTACHVGGGTWTCTAAT-3′), facilitating targeted amplification. Detection of the PCR amplification products was carried out using 2 % agarose gel electrophoresis, and the AxyPrep PCR Cleanup Kit was utilized for the recovery of the target fragments. The quantification of the purified PCR product was accomplished using the Quant-iT PicoGreen dsDNA Assay Kit, integrated within a Qbit Fluorescence Quantification System. This process necessitated a minimum library concentration of 2 nM or higher for successful analysis. Libraries that met the criteria for on-line sequencing (featuring non-reproducible index sequences) were diluted in a gradient, mixed based on the required sequencing volume, and denatured into single strands with NaOH prior to on-line sequencing, and then sequenced at 2 × 250 bp bipartite ends using the NovaSeq sequencer. Utilizing FLASH (v1.2.8) software, we merged the sequences into extended tags, relying on the overlapping nature of the bipartite sequences. We also eliminated the barcode and primer sequences that were introduced during library construction. Subsequently, Vsearch (v2.3.4) was employed to filter out any chimeras present in the dataset.

Following data preprocessing, Vsearch was utilized to identify clean tags, defining sequences with a similarity exceeding 97 %, and the best centroids (geometrically centred) sequences are selected as representative sequences. The alpha diversity indices, encompassing Observed_OTUs, Shannon, Simpson, Chao 1, and Goods_coverage, and beta diversity indices, specifically principal coordinate analysis (PCoA), were subjected to analysis utilizing QIIME (v1.8.0). These annotations were based on the Ribosomal Database Project and the NCBI-16 S database, aiming to identify the species for each representative sequence. To identify the most distinct biomarkers in each group, we conducted a linear discriminant analysis (LDA) effect size (LEfSe) analysis. This involved employing the nonparametric factorial Kruskal-Wallis sum-rank test, followed by the unpaired Wilcoxon rank-sum test. A LDA threshold of >5 was applied throughout the analysis. The phylogenetic investigation of communities by reconstruction of unobserved states (PICRUSt2) analysis of microbial functions of different bacterial communities according to kyoto encyclopedia of genes and genomes (KEGG) pathway at level III.

2.15. Untargeted and targeted metabolomics analysis

A 60 mg fecal sample was subjected to the addition of 600 μL of a 1:1 (v/v) methanol-water solution. A 40 mg eWAT was added 400 μL ultrapure water to homogenise and then take 200 μL of homogenate and add 800 μL of methanol/acetonitrile (v:v, 1:1). Fecal and eWAT samples were then vortexed with magnetic beads for homogenization. Subsequently, the sample was sonicated for 10 min at 4 °C. The samples were initially stored at −20 °C for a duration of 30 min, after which they were centrifuged at 14,500 rpm for 15 min at a temperature of 4 °C. Subsequently, 200 μL of the supernatant was dried using a vacuum centrifuge. Then, 200 μL of chromatography-grade methanol was added to the dried samples, which were vortexed for 2 min. This was followed by sonication in an ice bath and centrifugation to collect the supernatant samples.

The untargeted metabolome profiling of fecal samples was conducted employing the sophisticated UPLC-Orbitrap-MS/MS platform (Q-Exactive Focus, sourced from the USA). The raw data obtained was subsequently processed through the Compound Discoverer 2.1 software developed by Thermo Fisher Scientific (USA), leading to the derivation of retention time (RT), mass-to-charge ratios (m/z), and peak intensities. Metabolite identification was streamlined with the aid of the comprehensive mzCloud and mzVault databases. Additionally, statistical analyses encompassing principal component analysis (PCA), orthogonal partial least squares-discriminant analysis (OPLS-DA), and response substitution testing (RPT) were executed utilizing the SIMCA-P 14.1 software package (Umetrics, Umea, Sweden).

The metabolites of GA and amino acids of feces and eWAT were measured by targeted by metabolomics analysis, including protocatechuic acid, 4-*O*-methylgallic acid (4-*O*-MeGA), isoleucine, phenylalanine, tyrosine, tryptophan threonine, and serine. Stock solutions of 100 μg/mL of each metabolite were prepared by dissolving 1.0 mg of each metabolite in 10 mL of a 50:50 (v/v) methanol-water mixture. Then the standard solution was diluted in gradient to 10000, 5000, 2500, 1000, 500, 250, 100, 50, 25 ng/mL. For the quantification of metabolites, an external standard method was employed.

Briefly, the targeted quantitative results were first analyzed by Xcalibur software (version 3.0, Thermo Fisher, USA) to obtain information on mass (m/z), peaks, retention time and fragment ion intensity. The generated mass list was then used to establish peaks and calculate peaks, and finally analyzed qualitatively and quantitatively.

2.16. Statistical analysis

Unless otherwise specified, the data are presented as the mean values accompanied by their respective standard errors (SEM), with the numbers of mice indicated. The statistical analyses were all conducted with the aid of GraphPad Prism 8 software, employing an unpaired one-tailed *t*-test for comparisons for all data except for the difference between pathogenic and beneficial bacteria, which was done using the Mann-Whitney *U* test. Details of the biological replicates for each experiment can be found in the respective legends. Using PICRUSt2,

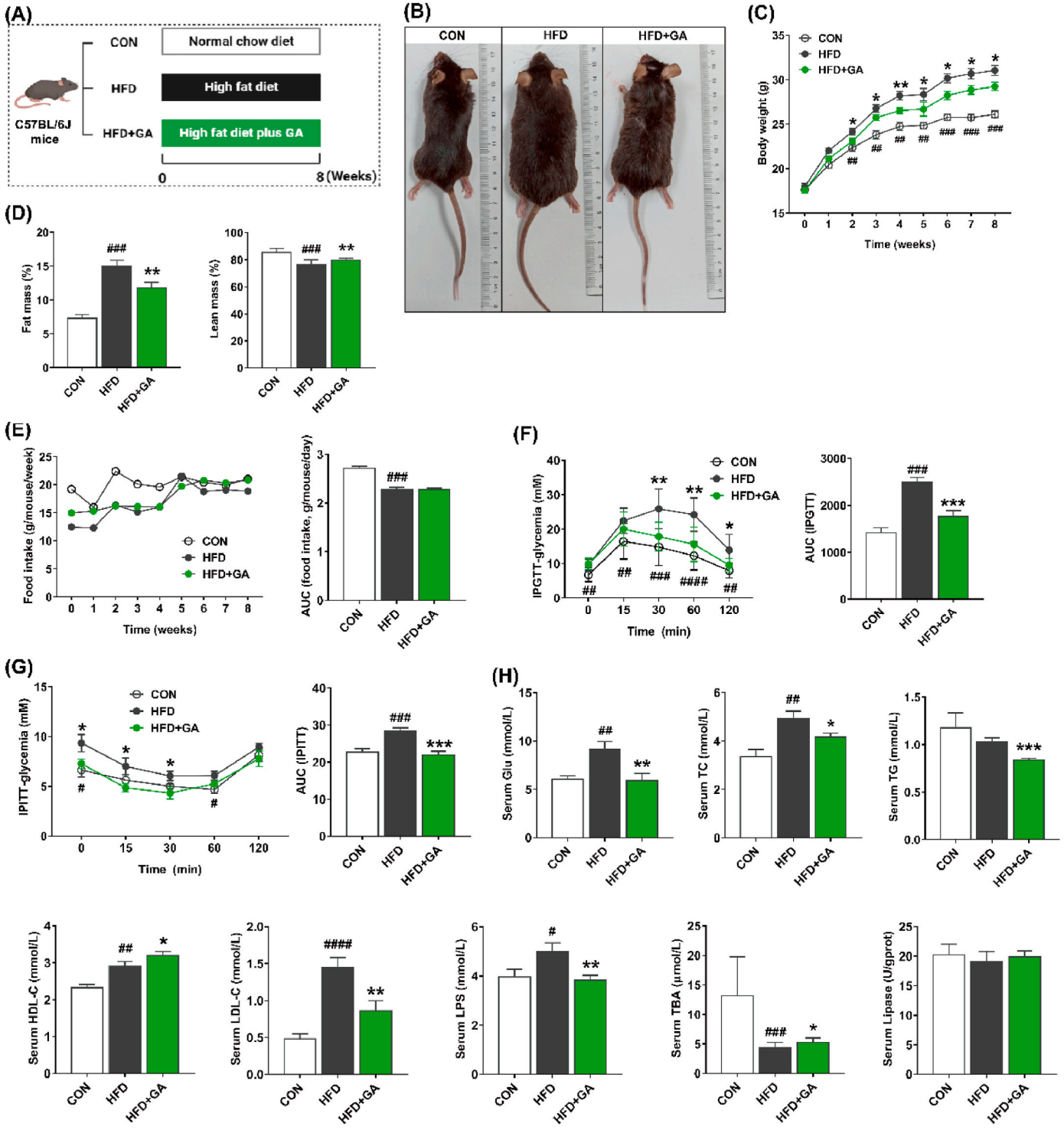

Fig. 1. GA reduced body weight and serum parameters in HFD-fed mice. (A) Schematic of experimental approach. (B) Images of representative mice. (C) Body weight of each group. (D) Body composition. (E) Food intake and its AUC. (F) The IPGTT and its AUC. (G) The IPITT and its AUC. (H) Concentrations of serum parameters, including Glu, TC, TG, HDL-C, LDL-C, LPS, TBA, and lipase. Data were presented in the format of mean ± SEM and were statistically evaluated using unpaired *t*-test, with data denoted as follows: *or #$P < 0.05$; **or ##$P < 0.01$; ***or ###$P < 0.001$. The mark # stands for comparison between the CON and HFD groups, while the mark * stands for comparison between the HFD and HFD + GA groups. CON = normal diet; HFD = high-fat diet; HFD + GA = high-fat diet plus 200 mg/kg body weight GA.

function prediction was performed. This was identified through statistical analysis of metagenomic profiles (STAMP) analysis, with a 95 % confidence interval applied (Wilcox test, $P < 0.05$). The relationships among the varying parameters were evaluated utilizing Spearman's correlation coefficient. To visualize these correlations and facilitate clustering, the OmicStudio platform available at https://www.omicstudio.cn was utilized for generating heatmaps and carrying out clustering procedures.

3. Results

3.1. GA reduced body weight and improved serum parameters in HFD-fed mice

Initially, we delved into the influence of GA on promoting body weight in mice subjected to HFD (Fig. 1A). Our findings unveiled a pronounced elevation in body weight among mice in HFD group, commencing from week 3, which was notably greater than both the CON group and HFD + GA group. This observation underscores the mitigating effect of GA on body weight in the context of HFD (Fig. 1B and C). Reduced fat mass and increased lean mass with GA supplementation (Fig. 1D). Furthermore, by week 5, both the HFD + GA and HFD groups attained a statistically significant peak in body weight, despite similar or lower food intake and its AUC value (Fig. 1E). In line with the body weight phenotype, the results of IPGTT and IPITT and their AUC values further confirmed that GA significantly improved impaired glucose tolerance status (Fig. 1F and G). Furthermore, the examination of serum biomarkers revealed a pronounced reduction in the concentrations of Glu, TG, TC, LDL-C, and LPS upon GA treatment, while the levels of HDL-C and TBA were significantly elevated in comparison to the HFD group (Fig. 1H). These findings implied the potential efficacy of GA in mitigating body weight gain in mice subjected to HFD, which was accompanied by favorable alterations in serum lipid parameters and glycemic status.

3.2. GA alleviated adipose accumulation in eWAT of HFD-fed mice

Our findings revealed a pronounced reduction in relative weight of eWAT within HFD + GA group compared to HFD group, accompanied by a significant elevation in iBAT levels relative to the latter. However, no discernible difference was observed in the indices of iWAT and pWAT between these two groups (Fig. 2A). Meanwhile, the eWAT cells in HFD + GA group had clearer boundaries, and the cell volume was significantly smaller than that in HFD group as shown by the quantitative results of H&E staining (Fig. 2B). Furthermore, when comparing HFD + GA group to HFD group, elevated levels of mRNA and protein expression were observed for UCP1, AdipoQ, and AdipoR2 (Fig. 2C and D). Both immunohistochemical and immunofluorescence analyses showed that GA resulted in the localization of UCP1, AdipoQ and AdipoR2 in eWAT and significantly increased the expression of UCP1, AdipoQ and AdipoR2 in eWAT (Fig. 2E). These data suggested that GA treatment reduced potential fat storage and decreased eWAT hypertrophy.

3.3. GA promoted iBAT thermogenesis in HFD-fed mice

To further investigate the relationship between body energy expenditure and iBAT thermogenesis in mice, iBAT and rectal temperatures were measured in the initial state or in the cold exposure state for 6 h. The results showed that the iBAT temperatures in the CON and HFD + GA groups were higher than that in the HFD group in both the initial and the cold exposure states (Fig. 3A). In addition, in the initial state, the rectal temperatures of the CON and HFD + GA groups were significantly lower and higher than those of the HFD group, respectively. However, in the cold exposure state, only HFD group had a significantly higher rectal temperature than the CON group (Fig. 3B). Further, mice were kept in separate metabolic chambers for 12 h to investigate the iBAT thermogenesis. Compared with the HFD group, mean EE was significantly higher in the CON and HFD + GA groups, accompanied by a decrease in RER (Fig. 3C and D). Expectedly, GA significantly upregulated the mRNA and protein expression of UCP-1 in iBAT (Fig. 3E and F). Collectively, these results indicated that GA was involved in brown adipocyte thermogenesis.

3.4. GA restored disturbed gut microbiota in HFD-fed mice

The intricate relationship between the gut microbiota and obesity and lipid metabolism is well recognized. In this study, we delved deeper into the colonic microbiota compositions by employing 16 S rRNA sequencing techniques (Fig. S2 and Fig. 4). Venn diagram analysis revealed a total of 9 common features that were present across all three groups, and 1772, 1766, and 2196 unique features in the CON, HFD, and HFD + GA groups, respectively (Fig. S2A). The CON group received higher values of Observed_OTUs index, Shannon index, and Chao 1 index than the HFD and HFD + GA groups, with no significant difference between HFD group and HFD + GA group (Fig. S2B–F). Meanwhile, no difference in the Simpson index and Goods_coverage among all groups. The PCoA analysis based on Bray-Curtis demonstrated a distinct clustering of gut microbiota composition between the CON and HFD groups, as well as between the HFD and HFD + GA groups (Fig. S2G–H).

Distinct variations in the overall microbial composition were observed among the three groups, spanning the phylum, family, and genus taxonomic levels. Firmicutes and Proteobacteria were the major phyla in three groups, and Proteobacteria and Deferribacterota enriched in HFD group, but not in the CON and HFD + GA groups (Fig. 4A). At the family level, HFD group had a higher relative abundance of Desulfovibrionaceae than that in the CON and HFD + GA groups (Fig. 4B). At the genus level, HFD group recruited more *Desulfovibrio*, while the CON and HFD + GA groups reversed this alteration (Fig. 4C). Moreover, *Lachnospiraceae_NK4A136_group*, *Clostridiales_unclassified*, and *Adlercreutzia* enriched in the CON group, but not in HFD group. Similarly, HFD + GA group increased the relative abundance of *Lachnospiraceae_NK4A136_group* ($P = 0.070$), *Clostridiales_unclassified*, *Adlercreutzia*, and *Oscillospira* compared to HFD group.

To identify the specific bacterial taxa associated with GA, we compared the colonic microbiota of mice in the HFD and HFD + GA groups using the LEfSe method (Fig. 4D). Consistent with the above-mentioned results, HFD elevated the relative abundance of *Desulfovibrio*, suggesting that *Desulfovibrio* might be a marker discriminating the HFD and HFD + GA groups. Moreover, the microbial function predicted by PICRUSt2 analysis showed that HFD group significantly increased the lipoic acid metabolism, taurine and hypotaurine metabolism, cellular antigens, amyotrophic lateral sclerosis, and arachidonic acid metabolism, while HFD + GA group up-regulated sphingolipid metabolism and biosynthesis of ansamycins (Fig. 4E). Collectively, GA restored structural and functional disturbances in the gut microbiota caused by HFD.

3.5. GA improved the gut microbiota metabolism in HFD-fed mice

Metabolomics is a comprehensive analysis of small molecules or metabolites that helps to unravel the pathogenesis of obesity. Based on this, we analyzed the metabolic patterns in mouse feces. Here, the PCA plot showed a clear separation between all groups (Fig. S3A). The degree of fit of OPLS-DA model (Fig. S3B) was validated by the permutation test (Fig. S3C), which indicated that the model was reliable and predictable and which further showed significant differences in fecal metabolites between the HFD and HFD + GA groups. Screening for fecal differential metabolites was based on the criteria of VIP >1 and $P < 0.05$, and 214 markers of fecal microbiota were identified between the HFD and HFD + GA groups (Fig. 5A). These differential metabolites, as shown in Fig. 5B and Table S4, primarily impact 13 metabolic pathways, including alpha-linolenic acid metabolism, alanine, aspartate and

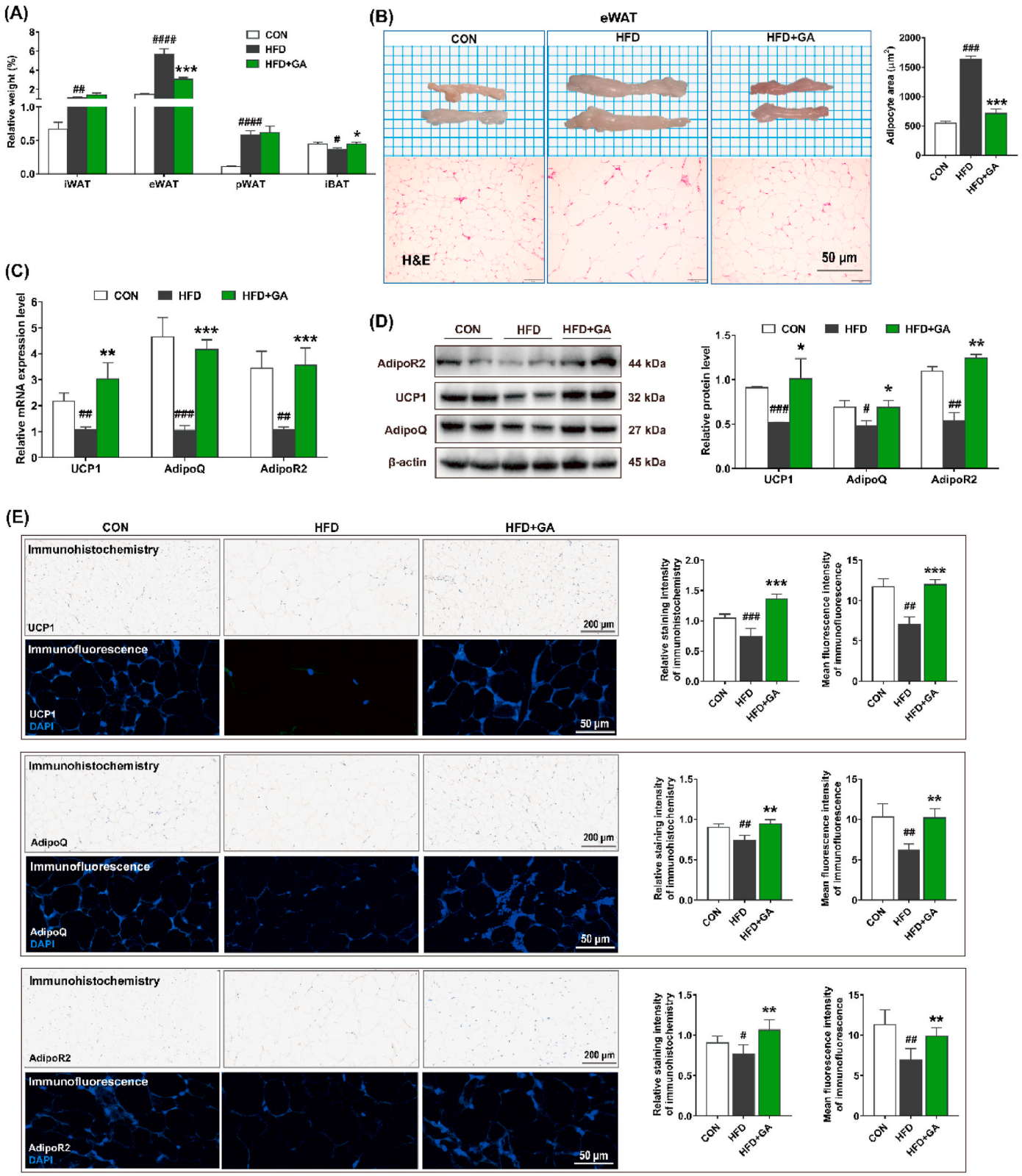

Fig. 2. GA prevented hypertrophy of eWAT in HFD-fed mice. (A) Relative weight of iWAT, eWAT, pWAT, and iBAT to body weight (%). (B) Representative images of eWAT and its H&E staining (Scale = 50 μm; n = 10) and adipocyte area. (C–D) The mRNA (n = 10) and protein (n = 4) expression levels of UCP1, AdipoQ, and AdipoR2 in eWAT, and both the mRNA and protein expression levels were normalized using β-actin. (E) Immunohistochemistry (Scale = 200 μm; n = 4) and immunofluorescence (Scale = 50 μm; n = 4) analysis and their quantitative results of UCP1, AdipoQ, and AdipoR2 in eWAT. Data were presented in the format of mean ± SEM and were statistically evaluated using unpaired *t*-test, with data denoted as follows: *or #$P < 0.05$; **or ##$P < 0.01$; ***or ###$P < 0.001$. The mark # stands for comparison between the CON and HFD groups, while the mark * stands for comparison between the HFD and HFD + GA groups. CON = normal diet; HFD = high-fat diet; HFD + GA = high-fat diet plus 200 mg/kg body weight GA.

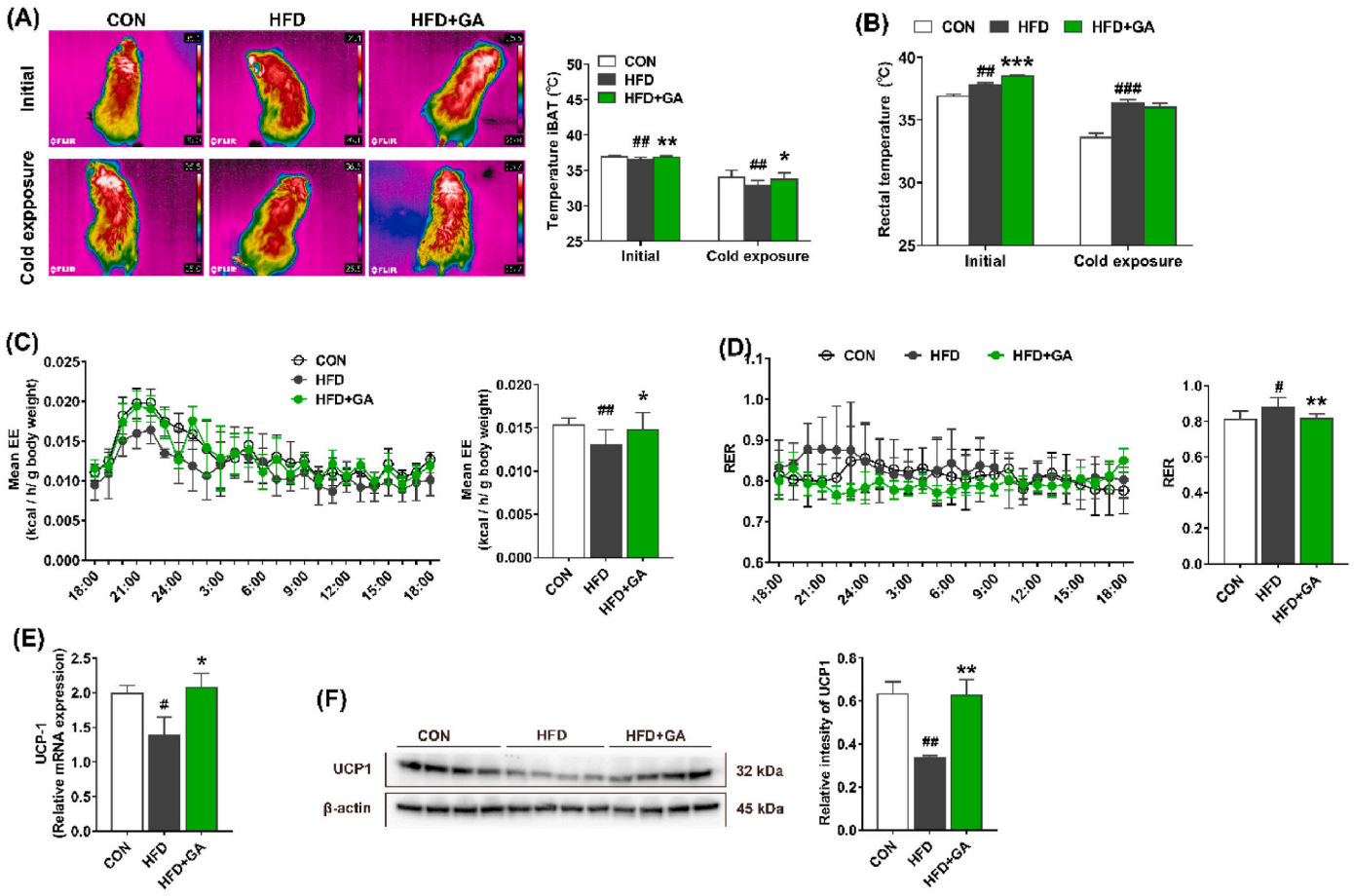

Fig. 3. GA promoted thermogenesis in HFD-fed mice. (A) Infrared images and iBAT region temperature measured at initial and cold exposure (n = 10). (B) Rectal temperature at initial and cold exposure (n = 10). (C–D) The mean energy expenditure and respiratory exchange ratio (n = 8). (E–F) The mRNA (n = 10) and protein (n = 4) expression levels of UCP1 in iBAT, and both the mRNA and protein expression levels were normalized using β-actin. Data were presented in the format of mean ± SEM and were statistically evaluated using unpaired *t*-test, with data denoted as follows: *or #$P < 0.05$; ##$P < 0.01$; ***$P < 0.001$. The mark # stands for comparison between the CON and HFD groups, while the mark * stands for comparison between the HFD and HFD + GA groups. CON = normal diet; HFD = high-fat diet; HFD + GA = high-fat diet plus 200 mg/kg body weight GA.

glutamate metabolism, and linoleic acid metabolism, and PPAR signaling pathway. Furthermore, among these metabolites, succinic acid, GA, garcinone E, 4-*O*-MeGA, and protocatechuic acid significantly increased, while palmitic acid decreased significantly in the fecal samples of HFD + GA group (Fig. 5C). Moreover, the targeted metabolomics analysis showed that amino acids, including isoleucine, phenylalanine, tyrosine, tryptophan, threonine, and serine in feces and eWAT showed no difference (Fig. S3D–E).

Next, Spearman's correlation analysis with $|r| > 0.6$ and $P < 0.01$ was performed to further explain the associations between different gut microbiota, fecal metabolites, serum parameters, body weight, and relative weight of eWAT. The results are shown in Fig. 5D and Table S5, and showed that *Desulfovibrio* appears to be involved in increasing serum LPS, LDL-C, TG, and relative weight of eWAT. Conversely, *Adlercreutzia* was involved in decreasing serum Glu, *Oscillospira* was involved in decreasing serum LPS and TG and relative weight of eWAT. Meanwhile, fecal palmitic acid was positively related to serum Glu and relative weight of eWAT. Additionally, fecal succinic acid showed a negative correlation with serum TC, LDL-C, and Glu. Similarly, fecal garcinone E was negatively correlated with serum LPS, LDL-C, and TG, body weight and relative weight of eWAT. The GA in feces showed benefit to decrease serum Glu and TG and relative weight of eWAT. Fecal 4-*O*-MeGA was negatively correlated with serum TC, LDL-C, Glu, and TG, body weight, and relative weight of eWAT. Fecal protocatechuic acid may exert serum Glu and TG-lowering effects and decrease relative weight of eWAT. Next, the targeted metabolomics in feces and eWAT showed that 4-*O*-MeGA and protocatechuic acid were significantly higher in HFD + GA group compared to HFD group (Fig. 5E). However, the targeted metabolomics analysis demonstrated that GA had no effect on amino acids in feces and eWAT (Fig. S3D–E). Collectively, these data revealed that GA may regulate lipid metabolism in obese mice by mediating gut microbiota and metabolites.

3.6. *Depletion of gut microbiota abrogated the anti-obesity effect of GA in HFD-fed mice*

To further understand the effect of gut microbiota on the anti-obesity effects of GA, mice maintained on HFD were treated for 8 weeks with either GA alone or GA and antibiotics therapy (Fig. 6A). The DNA in mouse feces could be reduced to 38 % by oral antibiotics (Fig. 6B), indicating successful clearance of gut microbiota. As shown in Fig. 6C–F, body weight, body composition (i.e., fat mass and lean mass), and food intake among the three groups were observed no significant differences. Additionally, the results of IPGTT and IPITT and their AUC values did not differ among all groups (Fig. 6G and H), confirming that the depletion of gut microbiota hinders the anti-obesity effects of GA. Correspondingly, serum Glu, TG, TC, LDL-C, HDL-C, LPS and TBA did not differ among three groups (Fig. 6I). Next, we found that the adipose tissue indexes (i.e., iWAT, eWAT, pWAT, and iBAT) had no significant difference among the groups (Fig. 6J).

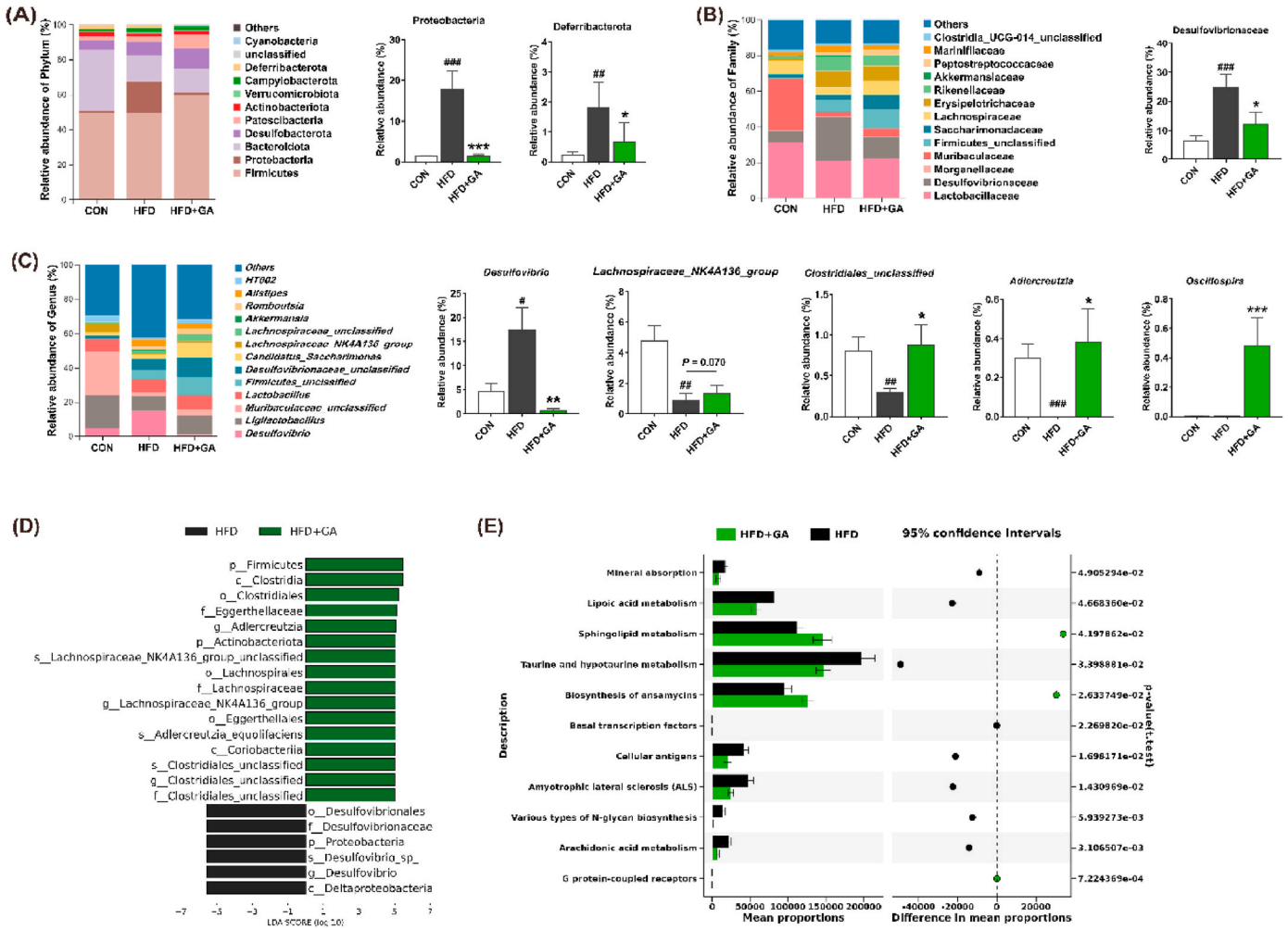

Fig. 4. GA modulated the composition of gut microbiota in HFD-fed mice. (A–C) Histogram of relative abundance of bacteria at the phylum, family, and genus levels. (D) LDA scores of differentially abundant OTUs among different groups using LEfSe (OTUs with a minimum relative abundance threshold of 0.01, LDA >5, and $P < 0.05$). (E) Prediction of gut microbiota functions predicted by PICRUSt2 analysis. Data were presented in the format of mean ± SEM and were statistically evaluated using Mann-Whitney *U* test, with data denoted as follows: *or #$P < 0.05$; **or ##$P < 0.01$; ***or ###$P < 0.001$. The mark # stands for comparison between the CON and HFD groups, while the mark * stands for comparison between the HFD and HFD + GA groups. CON = normal diet; HFD = high-fat diet; HFD + GA = high-fat diet plus 200 mg/kg body weight GA.

3.7. FMT from GA-treated mouse gut microbiota improved body weight and serum parameters in HFD-fed mice

Based on the above results, we conducted a 6-week FMT experiment, in which mice received fecal slurry from HFD or HFD + GA donor mice (Fig. 7A). The DNA in mouse feces could be reduced to 44 % by oral antibiotics (Fig. 7B), indicating successful clearance of gut microbiota. With no difference in feed intake, mice in the FMT-HFD + GA group outweighed those in the FMT-HFD group at week 4 and the difference was statistically significant. Thereafter, at weeks 6, 7, and 8, there was a trend towards a difference in body weights of the mice between the two groups, with p-values of 0.076, 0.068, and 0.096, respectively (Fig. 7C–E). In line with the body weight phenotype, the results of IPGTT and IPITT and their AUC values further confirmed that fecal slurry from HFD + GA donor mice significantly improved impaired glucose tolerance status (Fig. 7F and G). In addition, serum biomarker assays showed that after transplantation of feces from HFD + GA donor mice, concentrations of Glu, TG, TC, LDL-C, and LPS were significantly lower, whereas levels of HDL-C and TBA were significantly higher compared to the HFD group (Fig. 7H). The findings suggested that GA-treated mouse gut microbiota effectively reduced body weight of HFD-fed mice, and the effect of GA in suppressing weight gain was closely related to gut microbiota.

3.8. FMT from GA-treated mouse gut microbiota restored the disturbed gut microbiota and altered the metabolism in HFD-fed mice

Next, we also delved into the composition of the colonic microbiota using 16 S rRNA sequencing (Fig. S4 and Fig. 8). The alpha diversity, including Observed_OTUs index, Shannon index, Simpson index, Chao 1 index, Pielou_e index, and Goods_coverge showed no significant difference between the two groups (Fig. S4A). The PCA and PCoA analysis demonstrated a distinct clustering of gut microbiota composition between the two groups (Fig. S4B). At the phylum level, Desulfobacterota and Deferribacterota enriched in FMT-HFD group (Fig. 8A). At the family level, FMT-HFD group had a higher relative abundance of Desulfovibrionaceae than that in the FMT-HFD + GA group (Fig. 8B). At the genus level, FMT-HFD group recruited more *Desulfovibrio*, while the FMT-HFD + GA groups reversed this alteration (Fig. 8C). Moreover, FMT-HFD + GA group increased the relative abundance of *Lactobacillus*, *Adlercreutzia*, *Bifidobacterium*, and *Oscillospira* compared to FMT-HFD group. The PICRUSt2 analysis showed that FMT-HFD + GA group significantly increased the ubiquinone and other terpenoid-quinone biosynthesis and naphthalene degradation, while FMT-HFD group up-

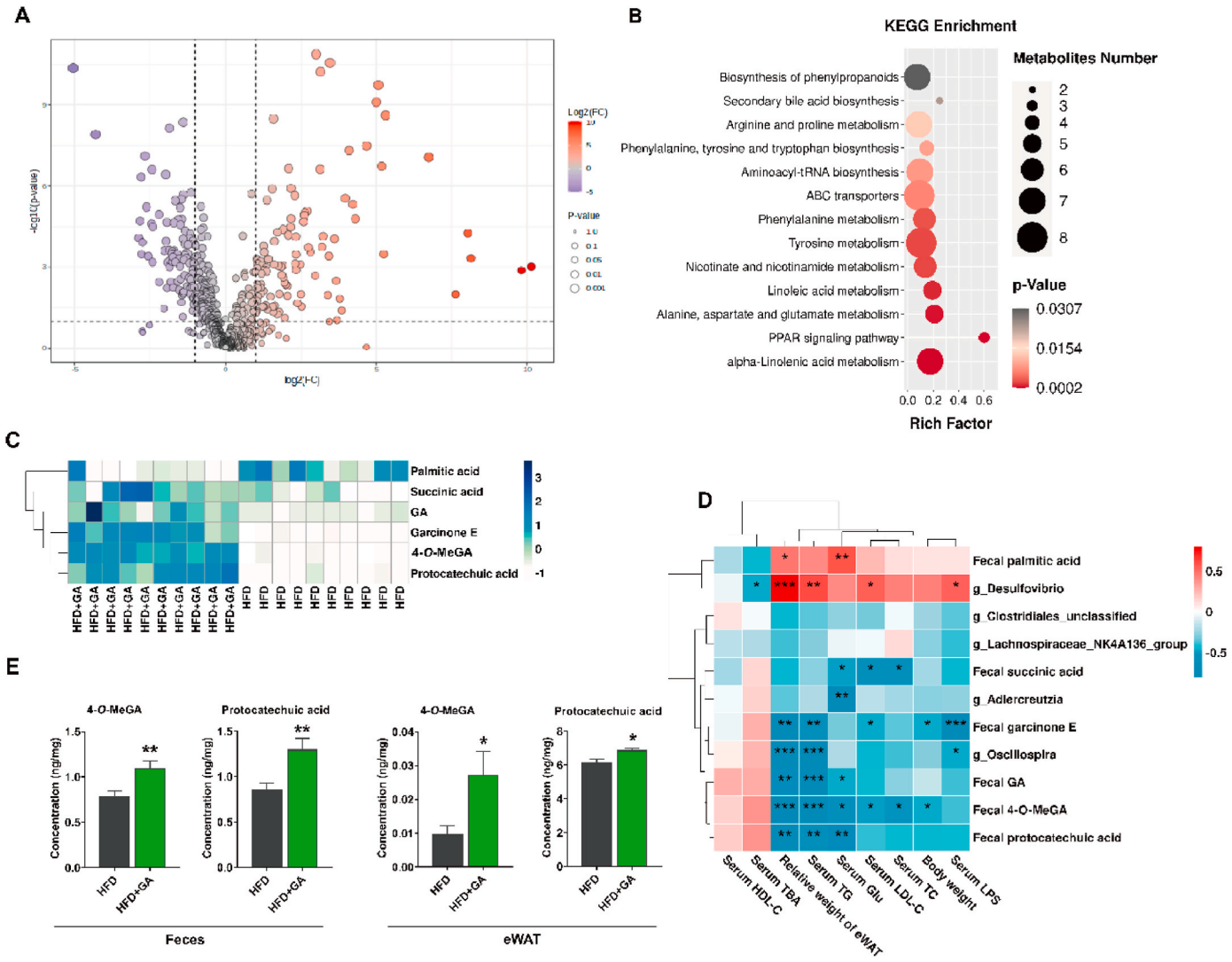

Fig. 5. GA regulated the metabolism in HFD-fed mice. (A) Volcano plots showing differential metabolites between the HFD and HFD + GA groups. (B) KEGG metabolic pathway enrichment analysis between the HFD and HFD + GA groups. (C) Heatmap analysis of fecal metabolites in the HFD and HFD + GA groups. (D) Spearman's correlation heatmap of differential gut microbiota, fecal metabolites, serum parameters, body weight, and relative weight of eWAT. (E) The quantitative values of 4-*O*-MeGA and protocatechuic acid in feces and eWAT analyzed by targeted metabolomics. Data were presented in the format of mean ± SEM and were statistically evaluated using unpaired *t*-test, with data denoted as follows: $^{*}P < 0.05$; $^{**}P < 0.01$; $^{***}P < 0.001$. HFD = high-fat diet; HFD + GA = high-fat diet plus 200 mg/kg body weight GA.

regulated the biosynthesis of ansamycins (Fig. 8D).

Similarly, we analyzed the metabolic patterns in mouse feces. the PCA (Fig. S4C), OPLS-DA (Fig. S4B), and permutation test (Fig. S4C) further showed significant differences in fecal metabolites between the two groups. Screening for fecal differential metabolites was based on the criteria of VIP >1 and $P < 0.05$, and 391 markers of fecal microbiota were identified (Fig. 8E). These differential metabolites mainly affect 20 metabolic pathways, including the PPAR signaling pathway, as shown in Fig. 8F and Table S6. Spearman's correlation analysis showed that one genus and four genera negatively and positively related to the obesity-related parameters, respectively (Fig. 8G and Table S7). Collectively, these data revealed that gut microbiota transplantation from GA-treated mice may regulate lipid metabolism in obese mice by mediating gut microbiota and metabolites.

3.9. FMT from GA-treated mouse gut microbiota attenuated fat accumulation of eWAT in HFD-fed mice

We found that the relative weight of iWAT, eWAT, and pWAT were significantly higher in FMT-HFD group compared to FMT-HFD + GA group, accompanied by a significant elevation in iBAT levels relative to the latter (Fig. 9A). Meanwhile, the eWAT cells in FMT-HFD + GA group had clearer boundaries, and the cell volume was significantly smaller than that in FMT-HFD group as shown by the quantitative results of H&E staining (Fig. 9B). Furthermore, elevated mRNA (Fig. 9C) and protein (Fig. 9D) expression levels of UCP1, AdipoQ, and AdipoR2 were observed in the FMT-HFD + GA group compared to the FMT-HFD group. These data suggested that GA-treated mouse gut microbiota reduced potential fat storage and decreased eWAT hypertrophy.

3.10. FMT from GA-treated mouse gut microbiota stimulated iBAT thermogenesis in HFD-fed mice

To further investigate the relationship between body energy expenditure and iBAT thermogenesis in mice, iBAT and rectal temperatures were measured in the initial state or in the cold exposure state for 6 h. The results showed that the iBAT temperature of the FMT-HFD + GA group was higher than that of the FMT-HFD group in both the initial

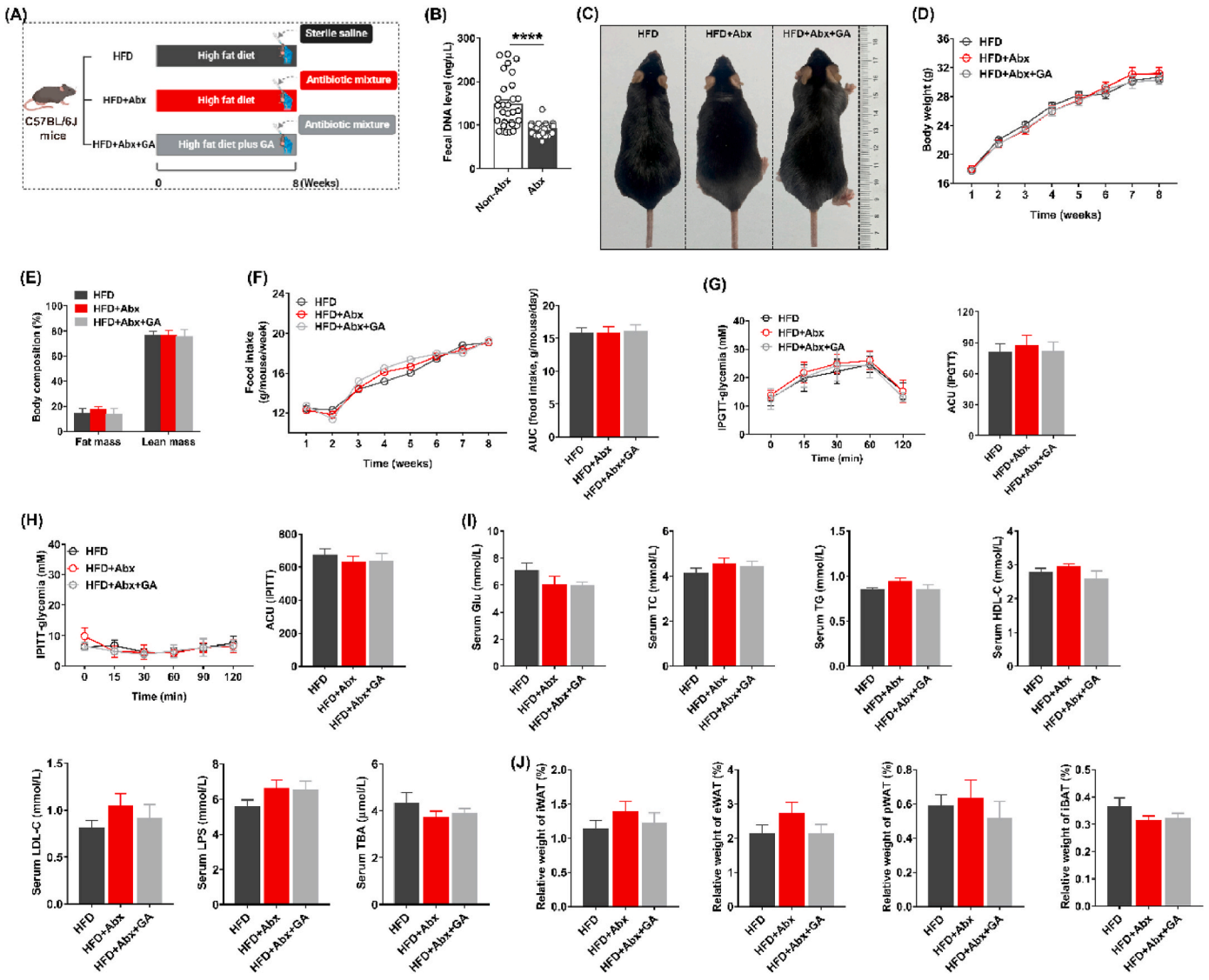

Fig. 6. Depletion of gut microbiota hindered anti-obesity effects of GA in HFD-fed mice. (A) Schematic of experimental approach. (B) Fecal DNA levels after 14 days of antibiotics treatment (n = 30 mice/group). (C) Images of representative mice. (D) Body weight of each group. (E) Body composition. (F) Food intake and its AUCs. (G) The IPGTT and its AUCs. (H) The IPITT and its AUCs. (I) Serum parameters. (J) The relative weight of iWAT, eWAT, pWAT, and iBAT. Data were presented in the format of mean ± SEM and were statistically evaluated using unpaired *t*-test, with data denoted as follows: ****$P < 0.0001$. HFD = high-fat diet; HFD + Abx = high-fat diet plus antibiotics treatment; HFD + Abx + GA = high-fat diet plus antibiotics with 200 mg/kg body weight GA.

state and the cold exposure state (Fig. 10A). In addition, the rectal temperature in the FMT-HFD + GA group was significantly higher than that in the FMT-HFD group in both the initial and cold exposure states (Fig. 10B). Further, mice were kept separate metabolic chambers for 12 h to investigate the iBAT thermogenesis. The mean EE was significantly increased in the FMT-HFD + GA group compared to the FMT-HFD group, while the RER was decreased (Fig. 10C and D). Expectedly, gut microbiota from GA-treated mice significantly upregulated the mRNA and protein expression of UCP-1 in iBAT (Fig. 10E and F). Taken together, these results suggested that FMT from the GA-treated gut microbiota played an important role in thermogenesis in mouse iBAT.

4. Discussion

Epidemiological research has underscored the pivotal function of gut microbiota in alleviating obesity and its accompanying metabolic abnormalities via multifaceted mechanisms (de Vos et al., 2022; Wang et al., 2024), while polyphenols have been shown to benefit gut microbiota dysbiosis induced by HFD (Liu et al., 2020). Despite the fact that numerous studies have highlighted the anti-obesity capabilities of GA (Paraíso et al., 2019b; Park et al., 2016), the exact correlation between its obesity-combating effects and the gut microbiota remains an area of ongoing investigation and clarification. Our current findings suggested that GA has a significant role in reducing body weight, improving glucose absorption and lipid levels, and modulating adipose tissue properties in HFD mice. The anti-obesity activity of GA stems not only from its modulation of UCP1, AdipoQ, and AdipoR2 in eWAT, but also from its augmentation of non-shivering thermogenesis mediated by upregulation of UCP1 in iBAT. These effects were closely related to the modulation of gut microbiota composition. GA may exert anti-obesity effects by influencing processes such as fat metabolism, energy expenditure, and thermogenesis in iBAT through modulating the composition and function of the gut microbiota. In this way, our study pioneered and elucidated the fundamental dependence of the major anti-obesity functions of GA on the gut microbiota-adipose tissue axis.

Expanding scope of research emphasizes impact of gut microbiota on obesity, prompting the emergence of microbiota management as a novel anti-obesity strategy (Liu et al., 2021). Notably, FMT is an important tool

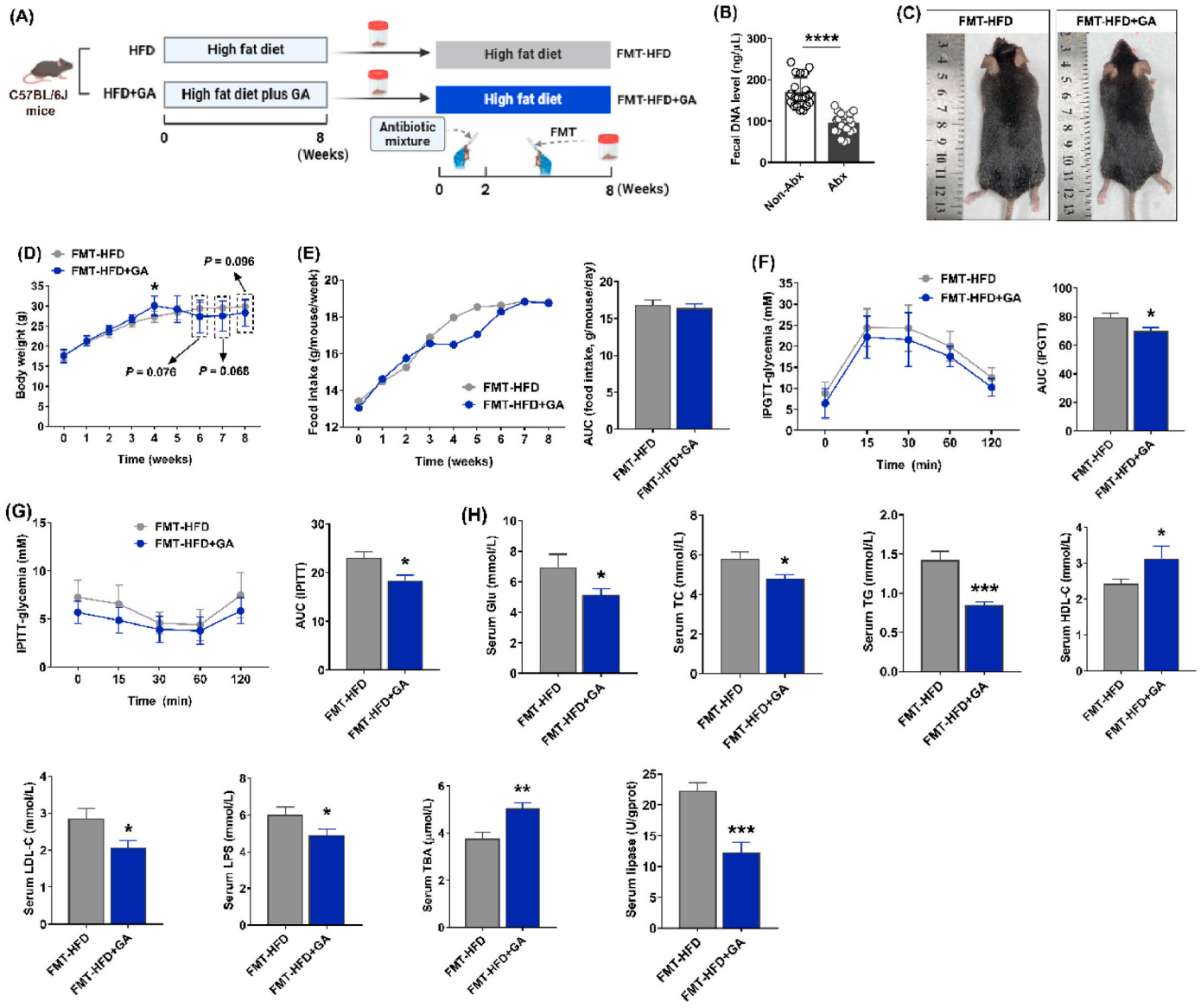

Fig. 7. Gut microbiota from GA-treated mice has an anti-obesity effect. (A) Schematic of experimental approach. (B) Fecal DNA levels after 14 days of antibiotics treatment (n = 20 mice/group). (C) Images of representative mice. (D) Body weight of each group. (E) Food intake and its AUC. (F) The IPGTT and its AUC. (G) The IPITT and its AUC. (H) Concentrations of serum parameters, including Glu, TC, TG, HDL-C, LDL-C, LPS, TBA, and lipase. Data were presented in the format of mean ± SEM and were statistically evaluated using unpaired *t*-test, with data denoted as follows: $^{*}P < 0.05$; $^{**}P < 0.01$; $^{***}P < 0.001$. FMT = fecal microbiota transplantation; FMT-HFD = receiving FMT from HFD; HFD = high-fat diet; FMT-HFD + GA = receiving FMT from HFD group plus 200 mg/kg body weight of GA.

for the treatment of gut microbiota-related diseases and an effective way to study the therapeutic effects of specific gut microbiota (Wang et al., 2020c). In the present study, FMT confirmed that GA acts as an anti-obesity agent by modulating gut microbiota. Our study found that a HFD reduced the diversity and disrupts the composition of the gut microbiota, whereas the direct addition of GA or FMT treatment counteracted these adverse effects, as evidenced by beta-diversity analysis. However, we noted that there was no difference in the alpha diversity of the overall microbiota between the direct addition of GA and after FMT treatment, suggesting that microbial colonization was not affected in the FMT experiment. In contrast, differences in gut microbiota composition and function prediction were observed between the donor mice with dietary intervention of GA and recipient mice with FMT. This may be due to biological differences between the mice used in the two experiments, especially differences in the structure of the natural gut microbiota (Peng et al., 2024). In particular, direct addition of GA and FMT drastically reduced the population of the pathogenic bacterium *Desulfovibrio*, which was positively associated with inflammation, obesity, and nonalcoholic fatty liver disease (NAFLD) (Lin et al., 2022; Xu et al., 2017) as evidenced by the fact that *Desulfovibrio* elevates TG, TC, LDL-C, and Glu, and decreases HDL-C (Li et al., 2020). Meanwhile, *Lachnospiraceae_NK4A136_group* and *Clostridiales_unclassified* significantly enriched by dietary intervention of GA, and *Lactobacillus* and *Bifidobacterium* were recruited by FMT treatment, and *Adlercreutzia* and *Oscillospira* were significantly elevated not only in direct addition of GA but also in FMT treatment. A synthesis of previous studies leads to the conclusion that these beneficial bacteria play a key role in maintaining intestinal health and ameliorating the symptoms of metabolic syndrome, such as obesity and NAFLD (Ma et al., 2020; Kaur and Dey, 2023; Yang et al., 2021; Oñate et al., 2023). Furthermore, PICRUSt analysis suggested that direct addition of GA and FMT enhanced metabolic activities critical for metabolic improvement. The possible mechanism is that GA inhibits bacterial growth and inhibits biofilm formation by altering membrane structure and bacterial metabolism (Keyvani Ghamsari et al.,

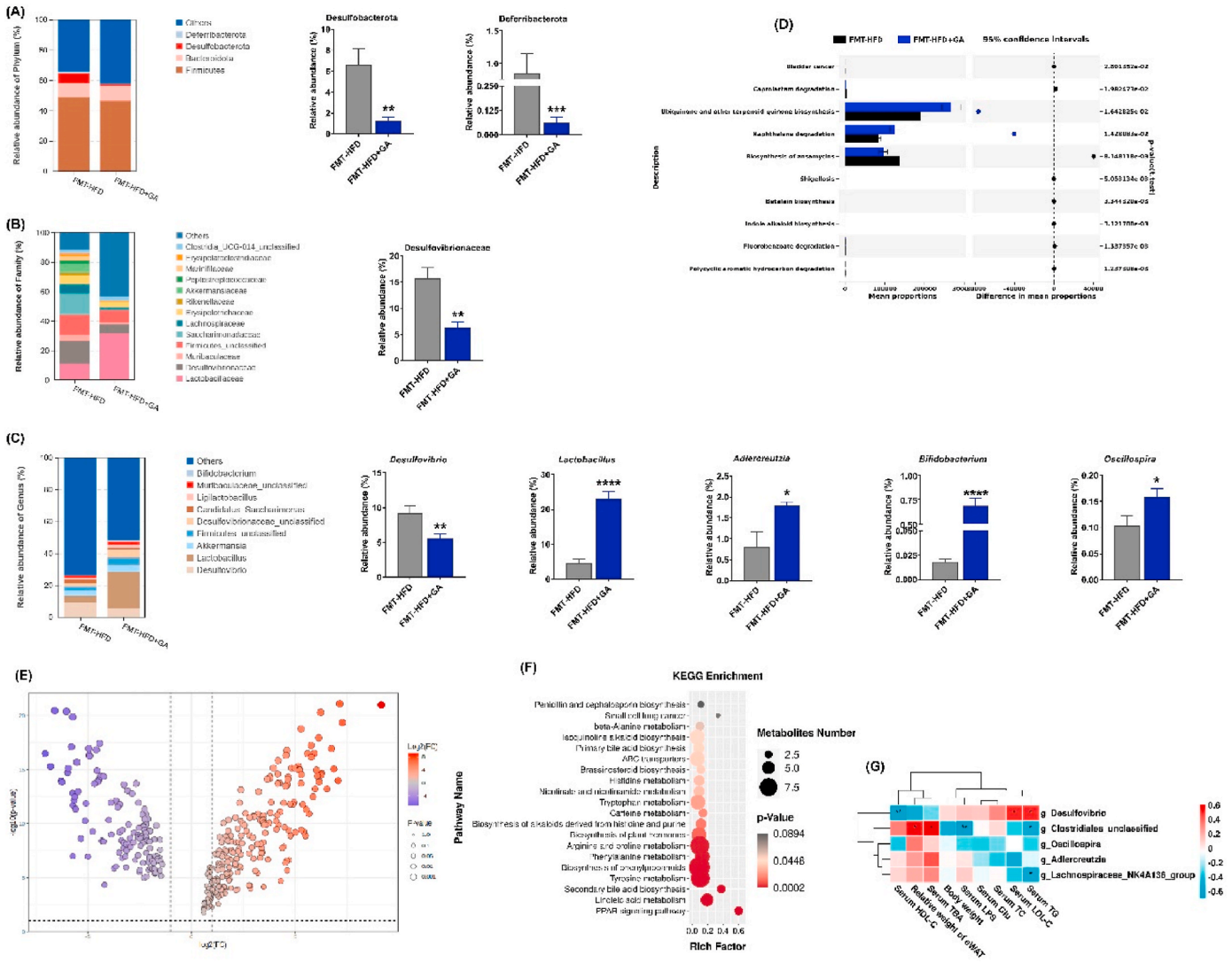

Fig. 8. Gut microbiota from GA-treated mice modulated the composition of gut microbiota and metabolism in HFD-fed mice. (A–C) Histogram of relative abundance of bacteria at the phylum, family, and genus levels. (D) Prediction of gut microbiota functions predicted by PICRUSt2 analysis. (E) Volcano plots showing differential metabolites between the FMT-HFD and FMT-HFD + GA groups. (F) KEGG metabolic pathway enrichment analysis between the FMT-HFD and FMT-HFD + GA groups. (G) Spearman's correlation heatmap of differential gut microbiota, serum parameters, body weight, and relative weight of eWAT. Data were presented in the format of mean ± SEM and were statistically evaluated using Mann-Whitney *U* test, with data denoted as follow: $^{*}P < 0.05$; $^{**}P < 0.01$; $^{***}P < 0.001$; $^{****}P < 0.0001$. FMT = fecal microbiota transplantation; FMT-HFD = receiving FMT from HFD; HFD = high-fat diet; FMT-HFD + GA = receiving FMT from HFD group plus 200 mg/kg body weight of GA.

2023). This can be seen by the up-regulation of sphingolipid metabolism and biosynthesis of ansamycins in the gut microbiota by GA, as well as by the fact that gut microbiota recruited by FMT treatment promote ubiquinone and other terpenoid-quinone biosynthesis and naphthalene degradation can be seen. Previous study has shown that increased sphingolipid metabolism is negatively associated with obesity, and that ansamycins exhibit antimicrobial activity and anti-inflammatory activity (Liu et al., 2024). Additionally, ubiquinone is an essential component of the electron transport chain in proteobacteria and eukaryotes (Abby et al., 2020), and up-regulation of naphthalene degradation is beneficial for the maintenance of intestinal homeostasis (Li et al., 2022). However, the exact reasons need to be further investigated.

A large number of metabolites originating from the gut microbiota play an important role in regulating the host's immune response (Yang and Cong, 2021), maintaining the integrity of the gut mucosa (Kim, 2018), managing glucose and lipid metabolism, and influencing insulin sensitivity (Bastos and Rangel, 2022). Such regulatory mechanisms contribute to the control of obesity (Agus et al., 2021). Our study found enrichment of succinic acid, gasserone E, protocatechuic acid, and 4-*O*-MeGA, as well as dilution of palmitic acid in the feces by the direct addition of GA.

Succinic acid counteracts the metabolic offset induced by a HFD (Liu et al., 2022), while gasserone E specifically inhibits fatty acid synthase activity (Liang et al., 2018), and administration of palmitic acid leads to persistent insulin resistance in pancreatic β-cells (Solinas et al., 2006). Therefore, increasing succinic acid and gathione E levels and decreasing palmitic acid levels could be a potential means of preventing and treating obesity. Notably, as major GA metabolites (Barnes et al., 2020), protocatechuic acid has been shown to counteract HFD-induced obesity and increase UCP1 levels in adipose tissue, thereby promoting thermogenesis (Xiang et al., 2023), whereas 4-*O*-MeGA may inhibit endothelial adhesion molecules (Lee et al., 2006) and expression of related inflammatory genes in *in vitro* cellular models (Na et al., 2006). These results suggested that GA has the ability to modulate metabolism in HFD-fed mice.

Based on the positive change in gut microbiota and metabolites, we

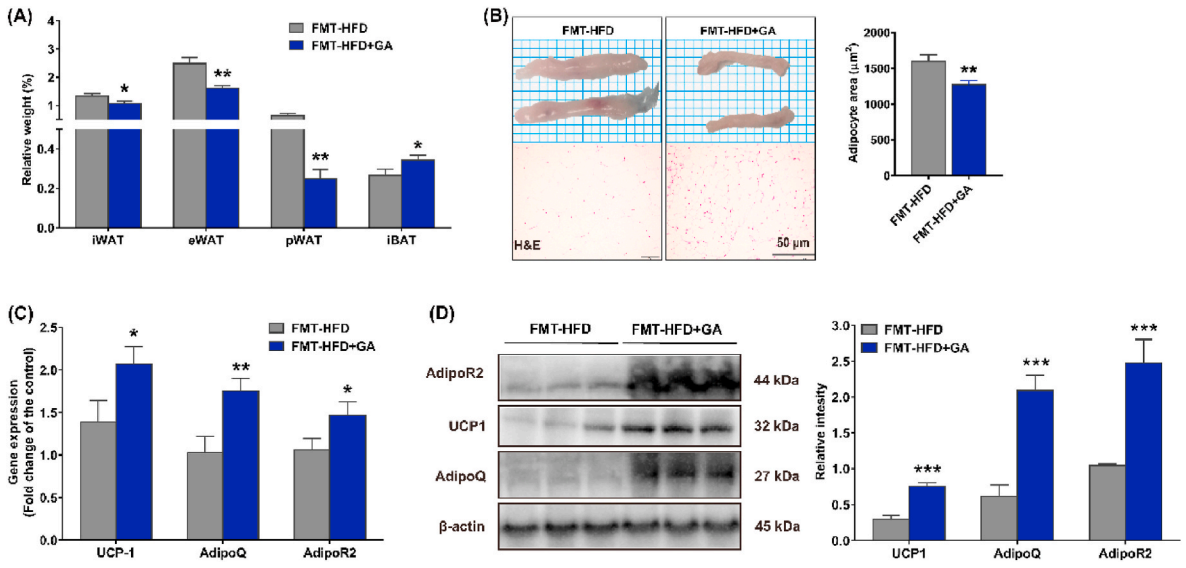

Fig. 9. Gut microbiota from GA-treated mice prevents hypertrophy of eWAT in HFD-fed mice. (A) Relative weight of iWAT, eWAT, pWAT, and iBAT to body weight (%). (B) Representative images of eWAT and its H&E staining (Scale = 50 μm; n = 10) and adipocyte area. (C–D) The mRNA (n = 10) and protein (n = 3) expression levels of UCP1, AdipoQ, and AdipoR2 in eWAT, and both the mRNA and protein expression levels were normalized using β-actin. Data were presented in the format of mean ± SEM and were statistically evaluated using unpaired *t*-test, with data denoted as follows: $^{*}P < 0.05$; $^{**}P < 0.01$; $^{***}P < 0.001$. FMT = fecal microbiota transplantation; FMT-HFD = receiving FMT from HFD; HFD = high-fat diet; FMT-HFD + GA = receiving FMT from HFD group plus 200 mg/kg body weight of GA.

continued to explore whether this change positively regulates energy metabolic function and adipogenesis in adipose tissue. Previous studies suggested that UCP1 induction in WAT facilitates non-shivering thermogenesis, a crucial mechanism for mammalian thermoregulation and fat mass reduction (Srivastava et al., 2020; Wang et al., 2022). Meanwhile, as a critical regulator of non-shivering thermogenesis in BAT, UCP1 mediates adaptive thermogenesis through its dual capacity to dissipate proton gradients and coordinate substrate oxidation in glucose/lipid metabolism (Wang et al., 2022). In this study, we found that dietary supplementation with GA and FMT significantly up-regulated UCP1 expression not only in eWAT but also in BAT, thereby promoted adipose tissue thermogenesis and energy expenditure. Constantly with our results, previous studies have pointed out that UCP1 stimulants can greatly contribute to our understanding of adipose tissue thermogenesis, including browning of WAT (Xu et al., 2024), and functional foods, food ingredients, and the gut microbiota are also commonly associated with the regulation and activation of UCP1 (Gong et al., 2024). Notably, the parallel elevation of fatty acid utilization (Li et al., 2023) and whole-body energy expenditure (Betz and Enerbäck, 2018) in both treatment modalities further demonstrates that UCP1 activation is a convergent node of metabolic regulation. Additionally, AdipoQ, the most abundant adipokine, is mainly produced by WAT, which mediates positive effects on whole-body metabolism by regulating relevant downstream signaling pathways (Gao et al., 2023). There is growing evidence that AdipoQ binds to its transmembrane receptor, AdipoR2, which is thought to play and its role in metabolism in the obese state (Sharma et al., 2023). This suggests that AdipoQ is a central regulator of metabolic homeostasis, accelerating glucose utilization (Scheurlen et al., 2022), promoting fatty acid oxidation, and inhibiting TG and TC synthesis to counteract obesity-associated pathologies (Kim et al., 2021; Sena et al., 2017). Our results also revealed that dietary supplementation with GA and FMT significantly up-regulated AdipoQ and AdipoR2 expression in eWAT. These beneficial changes decreased the eWAT weight, which supported the modulation of lipid metabolism of GA (Paraíso et al., 2019a). Since AdipoQ could modulate adipose tissue energy flux and insulin sensitivity through the AdipoQ/AdipoR2 signaling axis, which directly influences systemic glucose uptake and metabolic syndrome progression (Makihara et al., 2016; Cao et al., 2021). Overall, our results were consistent with previous findings which indicated that GA ameliorated IPGTT and IPITT in eWAT of HFD-fed mice (Doan et al., 2015; Tanaka et al., 2020), and further added to the mechanism by which GA could alleviate obesity.

Taken together, HFD-triggers gut microbiota dysbiosis in our study, marked by elevated pathogenic *Desulfovibrio* and diminished beneficial *Lactobacillus* and *Bifidobacterium*, correlating with adipose insulin resistance and metabolic dysfunction. Mechanistically, HFD-altered microbiota suppressed UCP1-mediated thermogenesis in iBAT and disrupted AdipoQ-driven fatty acid oxidation in eWAT via microbial metabolite modulation. Our findings revealed that GA counteracted HFD-induced metabolic perturbations through dual microbiota-centric pathways. Fist, GA restored microbial equilibrium and attenuated dysbiosis-associated metabolic anomalies. Further, GA reprogramed microbial metabolites by modulating metabolites associated with fat metabolism, such as elevation of succinate and gasserone E and reduction of palmitic acid, thereby optimizing lipid homeostasis. These actions converged on the microbiota-adipose tissue axis, upregulating UCP1 and AdipoQ/AdipoR2 to coordinately enhance BAT thermogenesis and WAT lipolysis. The FMT treatment confirmed GA-modulated microbiota transplantation replicates anti-obesity outcomes, including elevated energy expenditure, suppressed respiratory quotient, and activation of ubiquinone/sphingolipid pathways, underscoring the reliance of GA on functional microbial remodeling for therapeutic efficacy.

5. Conclusions

In conclusion, our current study highlighted the anti-obesity effects of GA on HFD-fed mice via the gut microbiota-adipose tissue axis. Microbiome analyses suggested that the anti-obesity effects of direct addition of GA and FMT treatments may result from inhibition of proliferation of obesity-causing bacteria (i.e., *Desulfovibrio*), promotion of proliferation of beneficial bacteria, and modulation of intestinal-derived metabolites associated with lipid metabolic pathways. These beneficial effects were feeding back into the optimization of the serum glycolipid profile, decreasing and increasing the relative weights of eWAT and iBAT, respectively, and ultimately reducing body weight. Mechanistically, gut microbiota was involved in GA upregulation of UCP1, AdipoQ, and AdipoR2 expression in eWAT and UCP1 expression in iBAT. Our

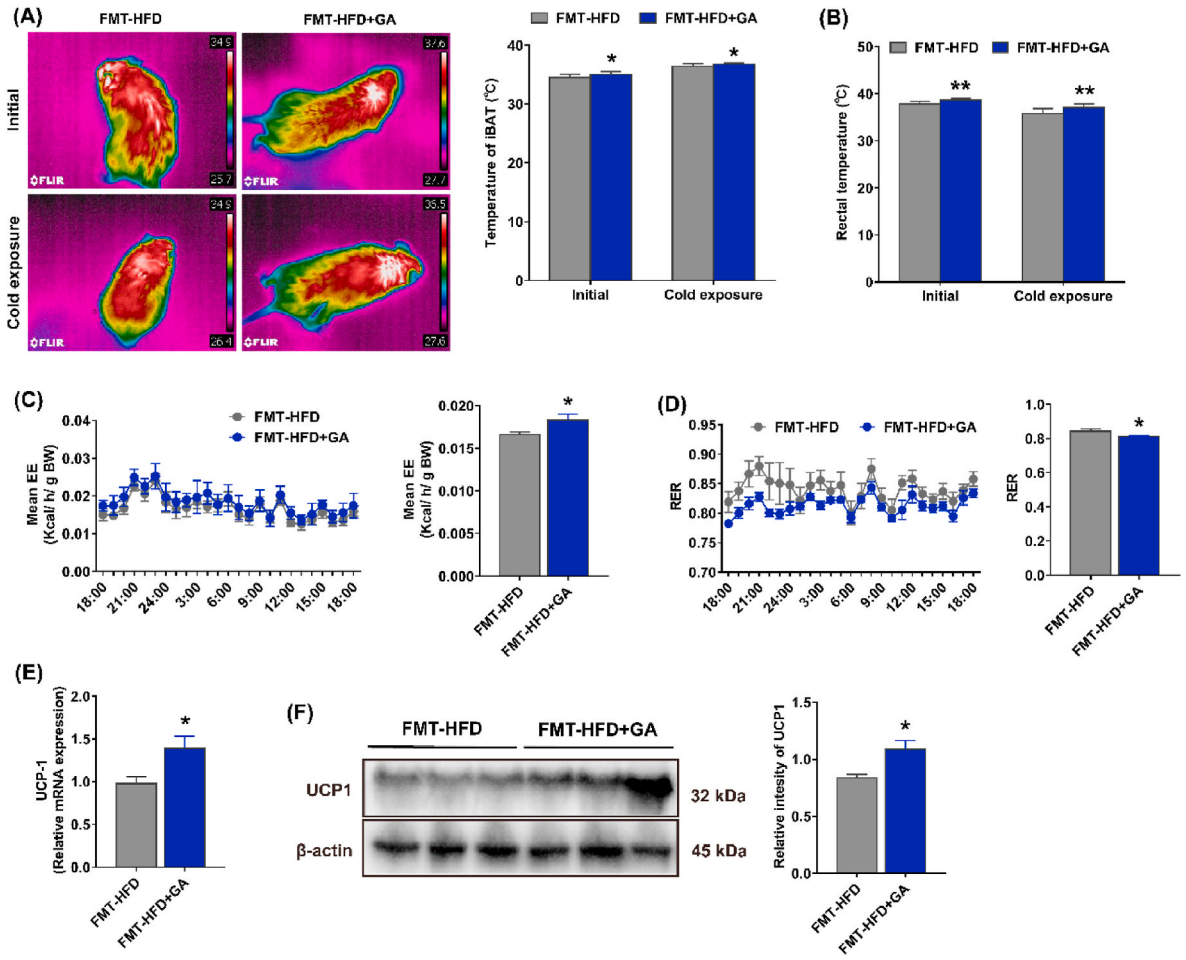

Fig. 10. Gut microbiota from GA-treated mice stimulated iBAT thermogenesis in HFD-fed mice. (A) Infrared images and iBAT region temperature measured at initial and cold exposure (n = 10). (B) Rectal temperature at initial and cold exposure (n = 10). (C) The mean energy expenditure (n = 8). (D) The respiratory exchange ratio (n = 8). (E–F) The mRNA (n = 10) and protein (n = 3) expression levels of UCP1 in iBAT, and both the mRNA and protein expression levels were normalized using β-actin. Data were presented in the format of mean ± SEM and were statistically evaluated using unpaired *t*-test, with data denoted as follows: $^{*}P < 0.05$; $^{**}P < 0.01$; $^{***}P < 0.001$. FMT = fecal microbiota transplantation; FMT-HFD = receiving FMT from HFD; HFD = high-fat diet; FMT-HFD + GA = receiving FMT from HFD group plus 200 mg/kg body weight of GA.

findings emphasized the critical role of GA in coordinating eWAT browning and iBAT thermogenesis through the gut microbiota. This highlighted the great potential of GA in the treatment of attenuating HFD-induced obesity by modulating the gut microbiota-adipose tissue axis.

CRediT authorship contribution statement

Shiyan Jian: Formal analysis, Investigation, Writing – original draft, Writing – review & editing. **Xiaoying Jian:** Formal analysis, Investigation, Writing – original draft. **Lan Ye:** Formal analysis, Investigation, Writing – original draft. **Kang Yang:** Investigation. **Limeng Zhang:** Investigation. **Yixuan Xie:** Investigation. **Jinping Deng:** Conceptualization, Supervision. **Yulong Yin:** Conceptualization, Supervision. **Baichuan Deng:** Conceptualization, Writing – review & editing, Funding acquisition.

Ethics approval statement

Ethical approval for all animal procedures detailed herein was granted by the Experimental Animal Ethics Committee of South China Agricultural University (Approval number: 2022F233). Animal experiments in this study complied with International Guiding Principles for Biomedical Research Involving Animals.

Funding

This study was supported by National Natural Science Foundation of China (Grant No. 32002186). The study was approved by the University review board.

Declaration of competing interest

The authors declare that they have no known competing financial interests or personal relationships that could have appeared to influence the work reported in this paper.

Acknowledgements

Not applicable.

Appendix A. Supplementary data

Supplementary data to this article can be found online at https://doi.org/10.1016/j.crfs.2025.101084.

Data availability

I have shared the link to my data/code at the Supplementary

Material file and the Data availability statement in the Manuscript.

References

Abby, S.S., Kazemzadeh, K., Vragniau, C., Pelosi, L., Pierrel, F., 2020. Advances in bacterial pathways for the biosynthesis of ubiquinone. Biochim. Biophys. Acta Bioenerg. 1861, 148259. https://doi.org/10.1016/j.bbabio.2020.148259.

Agus, A., Clement, K., Sokol, H., 2021. Gut microbiota-derived metabolites as central regulators in metabolic disorders. Gut 70, 1174–1182. https://doi.org/10.1136/gutjnl-2020-323071.

Bak, E., Kim, J., Jang, S., Woo, G., Yoon, H., Yoo, Y., et al., 2013. Gallic acid improves glucose tolerance and triglyceride concentration in diet-induced obesity mice. Scand. J. Clin. Lab. Investig. 73, 607–614. https://doi.org/10.3109/00365513.2013.831470.

Barcena, C., Valdes-Mas, R., Mayoral, P., Garabaya, C., Durand, S., Rodriguez, F., et al., 2019. Healthspan and lifespan extension by fecal microbiota transplantation into progeroid mice. Nat. Med. 25, 1234–1242. https://doi.org/10.1038/s41591-019-0504-5.

Barnes, R.C., Kim, H., Mertens-Talcott, S.U., Talcott, S.T., 2020. Improved recovery of galloyl metabolites from mango (Mangifera indica L.) in human plasma using protein precipitation with sodium dodecyl sulfate and methanol. Food Res. Int. 129, 108812. https://doi.org/10.1016/j.foodres.2019.108812.

Bastos, R.M., Rangel, É.B., 2022. Gut microbiota-derived metabolites are novel targets for improving insulin resistance. World J. Diabetes 13, 65–69. https://doi.org/10.4239/wjd.v13.i1.65.

Betz, M.J., Enerbäck, S., 2018. Targeting thermogenesis in brown fat and muscle to treat obesity and metabolic disease. Nat. Rev. Endocrinol. 14, 77–87. https://doi.org/10.1038/nrendo.2017.132.

Breton, J., Tennoune, N., Lucas, N., Francois, M., Legrand, R., Jacquemot, J., et al., 2016. Gut commensal *E. coli* proteins activate host satiety pathways following nutrient-induced bacterial growth. Cell Metab. 23, 324–334. https://doi.org/10.1016/j.cmet.2015.10.017.

Cao, E., Watt, M.J., Nowell, C.J., Quach, T., Simpson, J.S., De Melo Ferreira, V., et al., 2021. Mesenteric lymphatic dysfunction promotes insulin resistance and represents a potential treatment target in obesity. Nat. Metab. 3, 1175–1188. https://doi.org/10.1038/s42255-021-00457-w.

Chang, H., Chen, S., Lin, J., Chen, Y., Chen, Y., Liu, Y., et al., 2024. Phyllanthus emblica fruit improves obesity by reducing appetite and enhancing mucosal homeostasis via the gut microbiota-brain-liver axis in HFD-induced leptin-resistant rats. J. Agric. Food Chem. 72, 10406–10419. https://doi.org/10.1021/acs.jafc.4c01226.

Chao, J., Cheng, H., Chang, M., Huang, S., Liao, J., Cheng, Y., et al., 2021. Gallic acid ameliorated impaired lipid homeostasis in a mouse model of high-fat diet-and streptozotocin-induced NAFLD and diabetes through improvement of β-oxidation and ketogenesis. Front. Pharmacol. 11. https://doi.org/10.3389/fphar.2020.606759.

Clark, M., Centner, A.M., Ukhanov, V., Nagpal, R., Salazar, G., 2022. Gallic acid ameliorates atherosclerosis and vascular senescence and remodels the microbiome in a sex-dependent manner in ApoE−/− mice. J. Nutr. Biochem. 110, 109132. https://doi.org/10.1016/j.jnutbio.2022.109132.

Dalby, M.J., Ross, A.W., Walker, A.W., Morgan, P.J., 2017. Dietary uncoupling of gut microbiota and energy harvesting from obesity and glucose tolerance in mice. Cell Rep. 21, 1521–1533. https://doi.org/10.1016/j.celrep.2017.10.056.

de Vos, W.M., Tilg, H., Van Hul, M., Cani, P.D., 2022. Gut microbiome and health: mechanistic insights. Gut 71, 1020–1032. https://doi.org/10.1136/gutjnl-2021-326789.

Dludla, P.V., Nkambule, B.B., Jack, B., Mkandla, Z., Mutize, T., Silvestri, S., et al., 2018. Inflammation and oxidative stress in an obese state and the protective effects of gallic acid. Nutrients 11, 23. https://doi.org/10.3390/nu11010023.

Doan, K.V., Ko, C.M., Kinyua, A.W., Yang, D.J., Choi, Y., Oh, I.Y., et al., 2015. Gallic acid regulates body weight and glucose homeostasis through AMPK activation. Endocrinology 156, 157–168. https://doi.org/10.1210/en.2014-1354.

Dou, Z., Chen, C., Fu, X., Liu, R., 2022. A dynamic view on the chemical composition and bioactive properties of mulberry fruit using an *in vitro* digestion and fermentation model. Food Funct. 13, 4142–4157. https://doi.org/10.1039/D1FO03505C.

Gao, M., Cui, D., Xie, J., 2023. The role of adiponectin for immune cell function in metabolic diseases. Diabetes Obes. Metabol. 25, 2427–2438. https://doi.org/10.1111/dom.15151.

Gong, D., Lei, J., He, X., Hao, J., Zhang, F., Huang, X., et al., 2024. Keys to the switch of fat burning: stimuli that trigger the uncoupling protein 1 (UCP1) activation in adipose tissue. Lipids Health Dis. 23. https://doi.org/10.1186/s12944-024-02300-z.

González-Domínguez, Á., Domínguez-Riscart, J., Millán-Martínez, M., Lechuga-Sancho, A.M., González-Domínguez, R., 2023. Exploring the association between circulating trace elements, metabolic risk factors, and the adherence to a Mediterranean diet among children and adolescents with obesity. Front. Public Health 10, 1016819. https://doi.org/10.3389/fpubh.2022.1016819.

Guo, X., Luo, Y., Chen, L., Zhang, B., Chen, Y., Jia, D., 2022. Biomass antioxidant silica supported tea polyphenols with green and high-efficiency free radical capturing activity for rubber composites. Compos. Sci. Technol. 220, 109290. https://doi.org/10.1016/j.compscitech.2022.109290.

Huang, D., Chang, W., Yang, H., Wu, J., Shen, S., 2018. Gallic acid alleviates hypertriglyceridemia and fat accumulation via modulating glycolysis and lipolysis pathways in perirenal adipose tissues of rats fed a high-fructose diet. Int. J. Mol. Sci. 19, 254. https://doi.org/10.3390/ijms19010254.

Huber, L.C., Distler, O., Tarner, I., Gay, R.E., Gay, S., Pap, T., 2006. Synovial fibroblasts: key players in rheumatoid arthritis. Rheumatology 45, 669–675. https://doi.org/10.1093/rheumatology/kel065.

Jian, S., Yang, K., Zhang, L., Zhang, L., Xin, Z., Wen, C., et al., 2023. The modulation effects of plant-derived bioactive ingredients on chronic kidney disease: focus on the gut-kidney axis. Food Frontiers 4, 262–282. https://doi.org/10.1002/fft2.209.

Kaur, N., Dey, P., 2023. Bacterial exopolysaccharides as emerging bioactive macromolecules: from fundamentals to applications. Res. Microbiol. 174, 104024. https://doi.org/10.1016/j.resmic.2022.104024.

Keyvani Ghamsari, S., Rahimi, M., Khorsandi, K., 2023. An update on the potential mechanism of gallic acid as an antibacterial and anticancer agent. Food Sci. Nutr. 11, 5856–5872. https://doi.org/10.1002/fsn3.3615.

Kim, C.H., 2018. Microbiota or short-chain fatty acids: which regulates diabetes? Cell. Mol. Immunol. 15, 88–91. https://doi.org/10.1038/cmi.2017.57.

Kim, K., Kang, J.K., Jung, Y.H., Lee, S.B., Rametta, R., Dongiovanni, P., et al., 2021. Adipocyte PHLPP2 inhibition prevents obesity-induced fatty liver. Nat. Commun. 12. https://doi.org/10.1038/s41467-021-22106-2.

Lee, G., Na, H.J., Namkoong, S., Jeong, K.H., Han, S., Ha, K.S., et al., 2006. 4-*O*-methylgallic acid down-regulates endothelial adhesion molecule expression by inhibiting NF-kappaB-DNA-binding activity. Eur. J. Pharmacol. 551, 143–151. https://doi.org/10.1016/j.ejphar.2006.08.061.

Li, Y., Yang, Q., Shi, Z., Zhou, M., Yan, L., Li, H., et al., 2019. The anti-inflammatory effect of feiyangchangweiyan capsule and its main components on pelvic inflammatory disease in rats via the regulation of the NF-κB and BAX/BCL-2 pathway. Evid.-Based Complement Altern. Med. 2019, 1–11. https://doi.org/10.1155/2019/9585727.

Li, R., Yao, Y., Gao, P., Bu, S., 2020. The Therapeutic efficacy of curcumin *vs.* metformin in modulating the gut microbiota in NAFLD rats: a comparative study. Front. Microbiol. 11, 555293. https://doi.org/10.3389/fmicb.2020.555293.

Li, S., You, J., Wang, Z., Liu, Y., Wang, B., Du, M., et al., 2021. Curcumin alleviates high-fat diet-induced hepatic steatosis and obesity in association with modulation of gut microbiota in mice. Food Res. Int. 143, 110270. https://doi.org/10.1016/j.foodres.2021.110270.

Li, J., Zhao, Q., Huang, J., Jia, J., Zhu, T., Hong, T., et al., 2022. The functional microbiota of on- and off-year moso bamboo (Phyllostachys edulis) influences the development of the bamboo pest Pantana phyllostachysae. BMC Plant Biol. 22. https://doi.org/10.1186/s12870-022-03680-z.

Li, F., Zhang, F., Yi, X., Quan, L.L., Yang, X., Yin, C., et al., 2023. Proline hydroxylase 2 (PHD2) promotes brown adipose thermogenesis by enhancing the hydroxylation of UCP1. Mol. Metabol. 73, 101747. https://doi.org/10.1016/j.molmet.2023.101747.

Liang, Y., Luo, D., Gao, X., Wu, H., 2018. Inhibitory effects of garcinone E on fatty acid synthase. RSC Adv. 8, 8112–8117. https://doi.org/10.1039/c7ra13246h.

Lin, Y.C., Lin, H.F., Wu, C.C., Chen, C.L., Ni, Y.H., 2022. Pathogenic effects of *Desulfovibrio* in the gut on fatty liver in diet-induced obese mice and children with obesity. J. Gastroenterol. 57, 913–925. https://doi.org/10.1007/s00535-022-01909-0.

Lingvay, I., Sumithran, P., Cohen, R.V., le Roux, C.W., 2022. Obesity management as a primary treatment goal for type 2 diabetes: time to reframe the conversation. Lancet 399, 394–405. https://doi.org/10.1016/S0140-6736(21)01919-X.

Liu, J., He, Z., Ma, N., Chen, Z.Y., 2020. Beneficial effects of dietary polyphenols on high-fat diet-induced obesity linking with modulation of gut microbiota. J. Agric. Food Chem. 68, 33–47. https://doi.org/10.1021/acs.jafc.9b06817.

Liu, B., Liu, X., Liang, Z., Wang, J., 2021. Gut microbiota in obesity. World J. Gastroenterol. 27, 3837–3850. https://doi.org/10.3748/wjg.v27.i25.3837.

Liu, X., Chen, Y., Zhao, L., Tian, Q., DeAvila, J.M., Zhu, M., et al., 2022. Dietary succinate supplementation to maternal mice improves fetal brown adipose tissue development and thermogenesis of female offspring. J. Nutr. Biochem. 100, 108908. https://doi.org/10.1016/j.jnutbio.2021.108908.

Liu, Z., Sun, W., Hu, Z., Wang, W., Zhang, H., 2024. Marine streptomyces-derived novel alkaloids discovered in the past decade. Mar. Drugs 22, 51. https://doi.org/10.3390/md22010051.

Ma, L., Ni, Y., Wang, Z., Tu, W., Ni, L., Zhuge, F., et al., 2020. Spermidine improves gut barrier integrity and gut microbiota function in diet-induced obese mice. Gut Microbes 12, 1–19. https://doi.org/10.1080/19490976.2020.1832857.

Makihara, H., Koike, Y., Ohta, M., Horiguchi-Babamoto, E., Tsubata, M., Kinoshita, K., et al., 2016. Gallic acid, the active ingredient of terminalia bellirica, enhances adipocyte differentiation and adiponectin secretion. Biol. Pharm. Bull. 39, 1137–1143. https://doi.org/10.1248/bpb.b16-00064.

Mithul Aravind, S., Wichienchot, S., Tsao, R., Ramakrishnan, S., Chakkaravarthi, S., 2021. Role of dietary polyphenols on gut microbiota, their metabolites and health benefits. Food Res. Int. 142, 110189. https://doi.org/10.1016/j.foodres.2021.110189.

Muzurovic, E., Peng, C.C., Belanger, M.J., Sanoudou, D., Mikhailidis, D.P., Mantzoros, C. S., 2022. Nonalcoholic fatty liver disease and cardiovascular disease: a review of shared cardiometabolic risk factors. Hypertension 79, 1319–1326. https://doi.org/10.1161/HYPERTENSIONAHA.122.17982.

Na, H.J., Lee, G., Oh, H.Y., Jeon, K.S., Kwon, H.J., Ha, K.S., et al., 2006. 4-*O*-Methylgallic acid suppresses inflammation-associated gene expression by inhibition of redox-based NF-kappaB activation. Int. Immunopharmacol. 6, 1597–1608. https://doi.org/10.1016/j.intimp.2006.06.004.

Oñate, F.P., Chamignon, C., Burz, S.D., Lapaque, N., Monnoye, M., Philippe, C., et al., 2023. Adlercreutzia equolifaciens is an anti-inflammatory commensal bacterium with decreased abundance in gut microbiota of patients with metabolic liver disease. Int. J. Mol. Sci. 24, 12232. https://doi.org/10.3390/ijms241512232.

Paraíso, A.F., Sousa, J.N., Andrade, J.M.O., Mangabeira, E.S., Lelis, D.D.F., de Paula, A. M.B., et al., 2019a. Oral gallic acid improves metabolic profile by modulating SIRT1

expression in obese mice brown adipose tissue: a molecular and bioinformatic approach. Life Sci. 237, 116914. https://doi.org/10.1016/j.lfs.2019.116914.
Paraíso, A.F., Sousa, J.N., Andrade, J.M.O., Mangabeira, E.S., Lelis, D.D.F., de Paula, A. M.B., et al., 2019b. Oral gallic acid improves metabolic profile by modulating SIRT1 expression in obese mice brown adipose tissue: a molecular and bioinformatic approach. Life Sci. 237, 116914. https://doi.org/10.1016/j.lfs.2019.116914 (1973).
Park, B., Lee, S., Lee, B., Kim, I., Baek, N., Lee, T.H., et al., 2016. New ethanol extraction improves the anti-obesity effects of black tea. Arch Pharm. Res. (Seoul) 39, 310–320. https://doi.org/10.1007/s12272-015-0674-8.
Peng, J., Liu, T., Meng, P., Luo, Y., Zhu, S., Wang, Y., et al., 2024. Gallic acid ameliorates colitis by trapping deleterious metabolite ammonia and improving gut microbiota dysbiosis. mBio 15. https://doi.org/10.1128/mbio.02752-23.
Perdomo, C.M., Cohen, R.V., Sumithran, P., Clément, K., Frühbeck, G., 2023. Contemporary medical, device, and surgical therapies for obesity in adults. Lancet 401, 1116–1130. https://doi.org/10.1016/S0140-6736(22)02403-5.
Piché, M., Tchernof, A., Després, J., 2020. Obesity phenotypes, diabetes, and cardiovascular diseases. Circ. Res. 126, 1477–1500. https://doi.org/10.1161/CIRCRESAHA.120.316101.
Santos-Marcos, J.A., Perez-Jimenez, F., Camargo, A., 2019. The role of diet and intestinal microbiota in the development of metabolic syndrome. J. Nutr. Biochem. 70, 1–27. https://doi.org/10.1016/j.jnutbio.2019.03.017.
Scheurlen, K.M., Chariker, J.H., Kanaan, Z., Littlefield, A.B., George, J.B., Seraphine, C., et al., 2022. The NOTCH4-GATA4-IRG1 axis as a novel target in early-onset colorectal cancer. Cytokine Growth Factor Rev. 67, 25–34. https://doi.org/10.1016/j.cytogfr.2022.06.002.
Sena, C.M., Pereira, A., Fernandes, R., Letra, L., Seica, R.M., 2017. Adiponectin improves endothelial function in mesenteric arteries of rats fed a high-fat diet: role of perivascular adipose tissue. Br. J. Pharmacol. 174, 3514–3526. https://doi.org/10.1111/bph.13756.
Sharma, P., Bhandari, C., Agnihotri, N., 2023. Dietary n-3 and n-6 polyunsaturated fatty acids differentially modulate the adiponectin and leptinmediated major signaling pathways in visceral and subcutaneous white adipose tissue in high fat diet induced obesity in Wistar rats. Nutr. Res. 110, 74–86. https://doi.org/10.1016/j.nutres.2022.12.004.
Singh, A.K., Kumar, P., Mishra, S.K., Rajput, V.D., Tiwari, K.N., Singh, A.K., et al., 2024. A dual therapeutic approach to diabetes mellitus via bioactive phytochemicals found in a poly herbal extract by restoration of favorable gut flora and related short-chain fatty acids. Appl. Biochem. Biotechnol. 196, 6690–6715. https://doi.org/10.1007/s12010-024-04879-6.
Solinas, G., Naugler, W., Galimi, F., Lee, M.S., Karin, M., 2006. Saturated fatty acids inhibit induction of insulin gene transcription by JNK-mediated phosphorylation of insulin-receptor substrates. Proc. Natl. Acad. Sci. U. S. A. 103, 16454–16459. https://doi.org/10.1073/pnas.0607626103.
Srivastava, R.K., Moliner, A., Lee, E., Nickles, E., Sim, E., Liu, C., et al., 2020. CD137 negatively affects “browning” of white adipose tissue during cold exposure. J. Biol. Chem. 295, 2034–2042. https://doi.org/10.1074/jbc.AC119.011795.
Tanaka, M., Sugama, A., Sumi, K., Shimizu, K., Kishimoto, Y., Kondo, K., et al., 2020. Gallic acid regulates adipocyte hypertrophy and suppresses inflammatory gene expression induced by the paracrine interaction between adipocytes and macrophages *in vitro* and *in vivo*. Nutr. Res. 73, 58–66. https://doi.org/10.1016/j.nutres.2019.09.007.
Tian, L., Jin, T., 2016. The incretin hormone GLP-1 and mechanisms underlying its secretion. J. Diabetes 8, 753–765. https://doi.org/10.1111/1753-0407.12439.
Truong, V., Jeong, W., 2022. Antioxidant and anti-inflammatory roles of tea polyphenols in inflammatory bowel diseases. Food Sci. Hum. Wellness 11, 502–511. https://doi.org/10.1016/j.fshw.2021.12.008.
Umadevi, S., Gopi, V., Elangovan, V., 2014. Regulatory mechanism of gallic acid against advanced glycation end products induced cardiac remodeling in experimental rats. Chem. Biol. Interact. 208, 28–36. https://doi.org/10.1016/j.cbi.2013.11.013.
Wang, D., Xia, M., Yan, X., Li, D., Wang, L., Xu, Y., et al., 2012. Gut microbiota metabolism of anthocyanin promotes reverse cholesterol transport in mice via repressing miRNA-10b. Circ. Res. 111, 967–981. https://doi.org/10.1161/CIRCRESAHA.112.266502.
Wang, P., Li, D., Ke, W., Liang, D., Hu, X., Chen, F., 2020a. Resveratrol-induced gut microbiota reduces obesity in high-fat diet-fed mice. Int. J. Obes. 44, 213–225. https://doi.org/10.1038/s41366-019-0332-1.
Wang, P., Wang, J., Li, D., Ke, W., Chen, F., Hu, X., 2020b. Targeting the gut microbiota with resveratrol: a demonstration of novel evidence for the management of hepatic steatosis. J. Nutr. Biochem. 81, 108363. https://doi.org/10.1016/j.jnutbio.2020.108363.
Wang, P., Gao, J., Ke, W., Wang, J., Li, D., Liu, R., et al., 2020c. Resveratrol reduces obesity in high-fat diet-fed mice via modulating the composition and metabolic function of the gut microbiota. Free Radical Biol. Med. 156, 83–98. https://doi.org/10.1016/j.freeradbiomed.2020.04.013.
Wang, L., Qiu, Y., Gu, H., Gan, M., Zhu, Y., Zhu, K., et al., 2022. Regulation of adipose thermogenesis and its critical role in glucose and lipid metabolism. Int. J. Biol. Sci. 18, 4950–4962. https://doi.org/10.7150/ijbs.75488.
Wang, Y., He, F., Liu, B., Wu, X., Han, Z., Wang, X., et al., 2024. Interaction between intestinal mycobiota and microbiota shapes lung inflammation. Imeta. https://doi.org/10.1002/imt2.241.
Wu, Q., Liang, X., Wang, K., Lin, J., Wang, X., Wang, P., et al., 2021. Intestinal hypoxia-inducible factor 2α regulates lactate levels to shape the gut microbiome and alter thermogenesis. Cell Metab. 33, 1988–2003. https://doi.org/10.1016/j.cmet.2021.07.007.
Xiang, P., Du, Y., Chen, G., Mao, Y., Li, S., Li, Q., et al., 2023. Dietary achievable dose of protocatechuic acid, a metabolite of flavonoids, inhibits high-fat diet-induced obesity in mice. Mol. Nutr. Food Res. https://doi.org/10.1002/mnfr.202300451.
Xu, P., Hong, F., Wang, J., Cong, Y., Dai, S., Wang, S., et al., 2017. Microbiome remodeling via the montmorillonite adsorption-excretion axis prevents obesity-related metabolic disorders. EBioMedicine 16, 251–261. https://doi.org/10.1016/j.ebiom.2017.01.019.
Xu, C., Zhang, X., Wang, Y., Wang, Y., Zhou, Y., Li, F., et al., 2024. Dietary kaempferol exerts anti-obesity effects by inducing the browing of white adipocytes via the AMPK/SIRT1/PGC-1α signaling pathway. Curr. Res. Food Sci. 8, 100728. https://doi.org/10.1016/j.crfs.2024.100728.
Yang, W., Cong, Y., 2021. Gut microbiota-derived metabolites in the regulation of host immune responses and immune-related inflammatory diseases. Cell. Mol. Immunol. 18, 866–877. https://doi.org/10.1038/s41423-021-00661-4.
Yang, K., Zhang, L., Liao, P., Xiao, Z., Zhang, F., Sindaye, D., et al., 2020. Impact of gallic acid on gut health: focus on the gut microbiome, immune response, and mechanisms of action. Front. Immunol. 11, 580208. https://doi.org/10.3389/fimmu.2020.580208.
Yang, J., Li, Y., Wen, Z., Liu, W., Meng, L., Huang, H., 2021. Oscillospira - a candidate for the next-generation probiotics. Gut Microbes 13. https://doi.org/10.1080/19490976.2021.1987783.
Yang, K., Jian, S., Guo, D., Wen, C., Xin, Z., Zhang, L., et al., 2022a. Fecal microbiota and metabolomics revealed the effect of long-term consumption of gallic acid on canine lipid metabolism and gut health. Food Chem. X 15, 100377. https://doi.org/10.1016/j.fochx.2022.100377.
Yang, X., Yi, X., Zhang, F., Li, F., Lang, L., Ling, M., et al., 2022b. Cytochrome P450 epoxygenase-derived EPA and DHA oxylipins 17,18-epoxyeicosatetraenoic acid and 19,20-epoxydocosapentaenoic acid promote BAT thermogenesis and WAT browning through the GPR120-AMPKα signaling pathway. Food Funct. 13, 1232–1245. https://doi.org/10.1039/D1FO02608A.
Yin, J., Li, Y., Han, H., Chen, S., Gao, J., Liu, G., et al., 2018. Melatonin reprogramming of gut microbiota improves lipid dysmetabolism in high-fat diet-fed mice. J. Pineal Res. 65, e12524. https://doi.org/10.1111/jpi.12524.